TG 1167
SEPTEMBER 1971
Copy No. 2

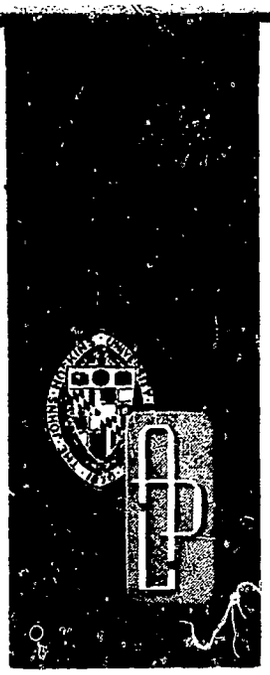

Technical Memorandum

THERMAL STRESS LIMITATIONS OF ALUMINA AND PYROCERAM 9606 A-SANDWICH RADOMES

by R. K. FRAZER

THE JOHNS HOPKINS UNIVERSITY ▪ APPLIED PHYSICS LABORATORY

82

UNCLASSIFIED
Security Classification

DOCUMENT CONTROL DATA - R & D

Security classification of title, body of abstract and indexing annotation must be entered when the overall report is classified)

1 ORIGINATING ACTIVITY (Corporate author)	2a. REPORT SECURITY CLASSIFICATION
The Johns Hopkins University Applied Physics Lab. 8621 Georgia Ave. Silver Spring, Md. 20910	Unclassified
	2b. GROUP NA

3 REPORT TITLE

Thermal Stress Limitations of Alumina and Pyroceram 9606 A-Sandwich Radomes

4 DESCRIPTIVE NOTES (Type of report and inclusive dates)

Technical Memorandum

5 AUTHOR(S) (First name, middle initial, last name)

R. K. Frazer

6 REPORT DATE	7a. TOTAL NO. OF PAGES	7b. NO. OF REFS
September 1971	69	24

8a. CONTRACT OR GRANT NO.	9a. ORIGINATOR'S REPORT NUMBER(S)
N00017-62-C-0604 b.	TG 1167
c. d.	9b. OTHER REPORT NO(S) (Any other numbers that may be assigned this report)

10. DISTRIBUTION STATEMENT

Approved for public release; distribution unlimited.

11. SUPPLEMENTARY NOTES	12. SPONSORING MILITARY ACTIVITY
	Naval Ordnance Systems Command

13. ABSTRACT

A study was made to define the flight limitations of supersonic missiles which are imposed by thermal stress failure of ceramic A-sandwich radome structures. The investigation verified the accuracy of an analytical model for determining thermal stresses in sandwich materials, and then used this model to define the thermal stress limits of alumina (Al_2O_3) and Pyroceram 9606 A-sandwich radomes when flown on supersonic trajectories. An investigation performed to determine the optimum A-sandwich dimensions for thermal stress resistance showed that there is no optimum sandwich configuration, but that the best choice is the monolithic wall. Velocity versus time plots of a number of A-sandwich wall configurations are presented, each showing the time of thermal stress failure for a particular trajectory. These give a representative picture of the flight limitations of alumina and Pyroceram 9606 A-sandwich radomes.

1a

DD FORM 1 NOV 65 1473

UNCLASSIFIED
Security Classification

14. KEY WORDS

Radome flight limits
Thermal stress
A-sandwich ceramics
Alumina
Pyroceram 9606
Porosity dependence of properties

TG 1167
SEPTEMBER 1971

Technical Memorandum

THERMAL STRESS LIMITATIONS OF ALUMINA AND PYROCERAM 9606 A-SANDWICH RADOMES

by R. K. FRAZER

THE JOHNS HOPKINS UNIVERSITY ▪ APPLIED PHYSICS LABORATORY
8621 Georgia Avenue, Silver Spring, Maryland 20910
Operating under Contract N00017-62-C-0604 with the Department of the Navy

THE JOHNS HOPKINS UNIVERSITY
APPLIED PHYSICS LABORATORY
SILVER SPRING, MARYLAND

ABSTRACT

A study was performed to define the flight limitations due to thermal stress failure of ceramic A-sandwich radome structures in supersonic missiles. The investigation was accomplished in two phases: The first phase verified the accuracy of an analytical model for determining thermal stresses in sandwich materials. The second phase used this analytical model to define the thermal stress limits of alumina (Al_2O_3) and Pyroceram 9606 A-sandwich radomes flown on supersonic trajectories.

Two steps were taken preliminary to the second phase of the investigation: The porosity dependence of the physical properties of alumina and Pyroceram were found, and an attempt was made to define the optimum A-sandwich wall dimensions for thermal stress resistance. The results of the optimization study showed that there is no optimum sandwich configuration for either alumina or Pyroceram 9606. It was shown that the best design for thermal stress resistance is the monolithic wall.

Subsequent to the optimization study, the thermal stress flight limitations were determined for many A-sandwich wall configurations. These limits take the form of velocity versus time plots on which the time of stress failure is plotted for a particular trajectory. While not every combination of trajectory and wall design was studied, the cases presented give a representative picture of the flight limitations of alumina and Pyroceram 9606 A-sandwich radomes.

CONTENTS

ILLUSTRATIONS

ILLUSTRATIONS (cont'd)

ILLUSTRATIONS (cont'd)

SYMBOLS

A	=	area perpendicular to heat flow direction
A' & b	=	empirical constants
c_p	=	specific heat
d	=	distance or diameter measurement
e	=	Naperian logarithm base
E	=	Young's modulus
G	=	shear modulus
K	=	bulk modulus
k	=	thermal conductivity
n	=	an index
P	=	bulk porosity
Q. E.	=	quadrant evaluation (launch angle)
q	=	heat flow rate
r	=	reflection coefficient
T	=	temperature
V	=	an element of volume, or velocity history
x	=	distance measurement
α	=	radiation heat transfer absorptivity
$\bar{\alpha}$	=	coefficient of linear thermal expansion

SYMBOLS (cont'd)

ϵ	=	emissivity or dielectric constant
θ	=	angle measurement
λ	=	wavelength
ν	=	Poisson's ratio
π	=	3.14159
ρ	=	density
σ	=	Stefan-Boltzman constant
τ	=	time
γ	=	geometrical factor of "effective radiation" conductivity

Subscripts

o, d	=	conditions at the dense (P = 0) state
a	=	reference to the material contained in pores (air or other gas)
P	=	conditions at a porous state
s	=	skin
c	=	core

SUMMARY

In recent years the idea of manufacturing ceramic radomes with sandwich type walls has been proposed to achieve electrical and mechanical advantages over monolithic designs. However, theoretical investigations have indicated that A-sandwich configurations will be more susceptible to thermal stress failures than monolithic walls. In an effort to validate this theoretical prediction, laboratory tests were conducted on several alumina (Al_2O_3) sandwich specimens to determine thermal stress failure levels. The test results showed low failure stresses and excellent correlation to the theoretical predictions.

Using the theoretical prediction method previously developed and verified, a study was performed wherein both alumina and Pyroceram 9606 A-sandwich radomes were flown on simulated trajectories. Variations of the core porosity and skin thickness were made to determine the optimum combination of these parameters for sustaining thermal stress. The flight simulations were run for walls that were electrically optimized for transmission at C-, X-, and K-band wavelengths. A knowledge of the porosity dependence of the physical properties of Pyroceram and alumina was required, and a preliminary study was performed to gather this information.

The study showed that there is no combination of core density and skin thickness which produces an optimum sandwich wall with respect to thermal stress resistance. The study also determined the environmental limits of A-sandwich alumina and Pyroceram 9606. A performance envelope with altitudes from 0 to 100 000 feet and speeds from 0 to 12 000 ft/s was used. In no case did any alumina A-sandwich design exceed a velocity of 4000 ft/s, and most of the cases studied had thermal stress failures near 2500 ft/s.

The highest limit is experienced for very thin K-band radomes and should not be taken as representative. K-band Pyroceram A-sandwich radomes achieved failures due to melting at 8000 ft/s while the majority of Pyroceram cases showed thermal stress failures in the range of 4500 to 5000 ft/s.

THE JOHNS HOPKINS UNIVERSITY
APPLIED PHYSICS LABORATORY
SILVER SPRING MARYLAND

1. INTRODUCTION

Early research and development by a few ceramic manufacturers (Refs. 1 through 4) led to the conclusion that A-sandwich radome structures would offer greater resistance to thermal stresses than monolithic designs, while providing lighter weight and broadband radar transmission. This conclusion was based largely on experimental work in which the thermal shock environment was vague and ill-defined.

In an effort to more quantitatively describe the thermal shock capability of A-sandwich configurations, a series of experimental and analytical studies were conducted at APL. The study had two major phases: The first phase dealt with correlating experimentally measured thermal stresses in alumina A-sandwich cylinders to a prediction method developed by Rivello (Ref. 5). The results of this test program demonstrated a high degree of correlation between the theoretically predicted and the experimentally measured stresses.

In the second phase, the theory of Rivello was used to generate thermal stress limits for A-sandwich radome structures. In order to accomplish this task efficiently, it was necessary to see if the design parameters (skin thickness, core density, and overall wall thickness) of A-sandwich walls could be optimized – that is, to see if there is an A-sandwich wall of a particular skin thickness (or core porosity) which resists thermal stresses better than all other walls. If such a design could be found, then fewer analyses would be required during the flight limitations study to define the maximum flight limits. The aerodynamic heating conditions experienced during supersonic flights are simulated analytically with a computer program developed by APL (Refs. 6 and 7). Two materials, 99.5% pure alumina (Al_2O_3) and Pyroceram 9606 ceramic are considered during this phase of the analysis. (Pyroceram 9606 is a registered trademark of Corning Glass.)

2. DISCUSSION OF INITIAL WORK

The initial interest in A-sandwich structures for missile applications grew out of work by the International Pipe and Ceramics Corporation in 1964. This company developed a slip casting technique for fabricating sandwich radome structures, carried out some qualitative thermal shock tests, and published a report of properties for alumina sandwich materials (Ref. 1).

In a paper given by Loyet (Ref. 2) at the 1964 OSU-RTD Symposium on Electromagnetic Windows, the thermal stress resistance of A-sandwich construction was claimed to be superior to all other types. This was based on the qualitative results of thermal stress experiments at Hughes Aircraft (Ref. 3).

In 1965, Corning Glass fabricated several small radomes of monolithic and A-sandwich alumina and used hot salt bath immersion for thermal shock testing. The findings of these tests were that monolithic radomes resisted thermal shock better than the A-sandwich designs. The tests lacked an adequate description of the thermal environment used and therefore no definitive conclusion can be reached.

Thermal shock tests were performed by Copeland and Greene (Ref. 4) on A-sandwich radomes in a molten metal bath. The bath temperatures were increased until immersion caused thermal stress failure. Some radomes survived bath temperatures of 2000°F to 2500°F, but all samples failed at 3000°F. Again, no quantitative definition of heat flux during the test is known, but the A-sandwich design was rated with a good thermal stress capability.

After a fabrication technique was developed for sandwich ceramics, and their use as radome materials was introduced, work began at APL toward developing an

cylindrical fixture known as a "clam shell," and the test cylinder was suspended concentrically in this divice (Fig. 1).

It was desirable to know the axial temperature distribution induced by the clam shell, so a sample cylinder was instrumented with an array of axial thermocouples and several tests were made to determine the magnitude and shape of the axial gradient under varying heating conditions. Figure 2 shows some representative data taken during these tests, and shows that the axial gradient is appreciable. In order to determine the effect of this axial temperature distribution on the stress distribution, a finite difference computer program was run under two cases: (1) with an axial variation in temperature and (2) with no axial variation in temperature. The computer results of the inner skin stresses at various points for the two cases are shown in Figs. 2 and 3. Inclusion of the axial gradient tends to reduce the high stresses near the ends of the cylinder, while at the same time the stresses at the center of the cylinder (which are of primary interest) are virtually unaffected. These results indicate that the test temperatures will cause the maximum stresses to occur at the middle section of the cylinder, which is most desirable.

The instrumentation for this test sequence consisted of high temperature biaxial strain gages (Budd Co. EC-124B-R2TS), temperature sensors (W. T. Bean Co. STG-50), and 40 gage iron constantan thermocouples (Thermoelectric Co.). Strain and temperature measurements were taken at the center station on the inner wall, and temperatures were measured at several outside locations. Figure 4 is a close-up view of the cylinder in the clam shell just prior to an application of black Rimshed-Mason paint. The paint was used to provide a high absorption surface. Two measurement locations were chosen for each cylinder at the middle station: one at an arbitrary 0° meridian and another 180° from this point. When all the instrumentation was installed, the cylinders were filled with fiberglass insulation and suspended on a metal rod by transite end closures as shown in Figs. 1 and 4. The insulation and sealing of the ends of the

analytical tool which could be used for predicting thermal stresses in sandwich structures. As a result of this effort, R. M. Rivello developed a theory for stresses in composite cylinders (Ref. 5) which was used to examine A-sandwich radome geometries on supersonic trajectories. Although Rivello's theory considers only cylindrical geometries, other work (Ref. 8) has shown that using the cylinder approximation to the radome shape is sufficiently accurate to make valid comparisons, and avoids the complexity involved with consideration of the actual radome contour.

The preliminary study using Rivello's theory showed that an A-sandwich wall will realize much higher tensile stresses (by a factor of about 3) than a monolithic wall in the same thermal environment. This result directly contradicted the earlier claims of good thermal stress resistance for A-sandwich walls. Because of this contradiction, the validity of Rivello's theory was questioned and an experimental program was initiated to determine the accuracy of the prediction method. The laboratory tests and subsequent comparisons to Rivello's theory constitute phase 1 of the current study and are discussed next.

3. VALIDATION OF STRESS PREDICTION METHOD

In order to validate the thermal stress theory of Rivello, two alumina A-sandwich cylinders were procurred from the Brunswick Corporation for the purpose of instrumentation and testing. Each cylinder was 10 inches long and had a 5-inch outside diameter. The overall wall thickness of the A-sandwich was about 0.5 inch, with skin thicknesses of about 0.02 inch. Inspection of the cylinders upon receipt revealed fair dimensional control; skin thickness variations were on the order of ±0.01 inch in 10 inches length, and overall wall thickness measurements varied ±0.017 inch from 0.452 inch. A complete dimensional survey was made and strength and density data were taken. A detailed report of these measurements can be found in Ref. 9. Briefly the results are:

Modulus of elasticity of skin	43.3×10^6 psi ±30%
Modulus of elasticity of core	1.99×10^6 psi ±33%
Modulus of rupture of skin	29 000 psi ±30%
Modulus of rupture of core	1200 psi ±15%
Poisson's ratio	0.24
Coefficient of thermal expansion for skin and core at 100°F	3.25×10^{-6} in/in-°F

In addition to these measurements, a cylinder which was not suitable for thermal shock tests was instrumented with strain gages and cut both axially and circumferentially to check for residual stresses caused during fabrication. The results of this investigation showed that negligible residual stresses were present in the cylinders.

Thermal stresses were induced in the test specimens by radiative heating. Twenty-four 12-inch, 2000-watt quartz lamps were arranged around a 12-inch diameter

cylindrical fixture known as a "clam shell," and the test cylinder was suspended concentrically in this divice (Fig. 1).

It was desirable to know the axial temperature distribution induced by the clam shell, so a sample cylinder was instrumented with an array of axial thermocouples and several tests were made to determine the magnitude and shape of the axial gradient under varying heating conditions. Figure 2 shows some representative data taken during these tests, and shows that the axial gradient is appreciable. In order to determine the effect of this axial temperature distribution on the stress distribution, a finite difference computer program was run under two cases: (1) with an axial variation in temperature and (2) with no axial variation in temperature. The computer results of the inner skin stresses at various points for the two cases are shown in Figs. 2 and 3. Inclusion of the axial gradient tends to reduce the high stresses near the ends of the cylinder, while at the same time the stresses at the center of the cylinder (which are of primary interest) are virtually unaffected. These results indicate that the test temperatures will cause the maximum stresses to occur at the middle section of the cylinder, which is most desirable.

The instrumentation for this test sequence consisted of high temperature biaxial strain gages (Budd Co. EC-124B-R2TS), temperature sensors (W. T. Bean Co. STG-50), and 40 gage iron constantan thermocouples (Thermoelectric Co.). Strain and temperature measurements were taken at the center station on the inner wall, and temperatures were measured at several outside locations. Figure 4 is a close-up view of the cylinder in the clam shell just prior to an application of black Rimshed-Mason paint. The paint was used to provide a high absorption surface. Two measurement locations were chosen for each cylinder at the middle station: one at an arbitrary 0° meridian and another 180° from this point. When all the instrumentation was installed, the cylinders were filled with fiberglass insulation and suspended on a metal rod by transite end closures as shown in Figs. 1 and 4. The insulation and sealing of the ends of the

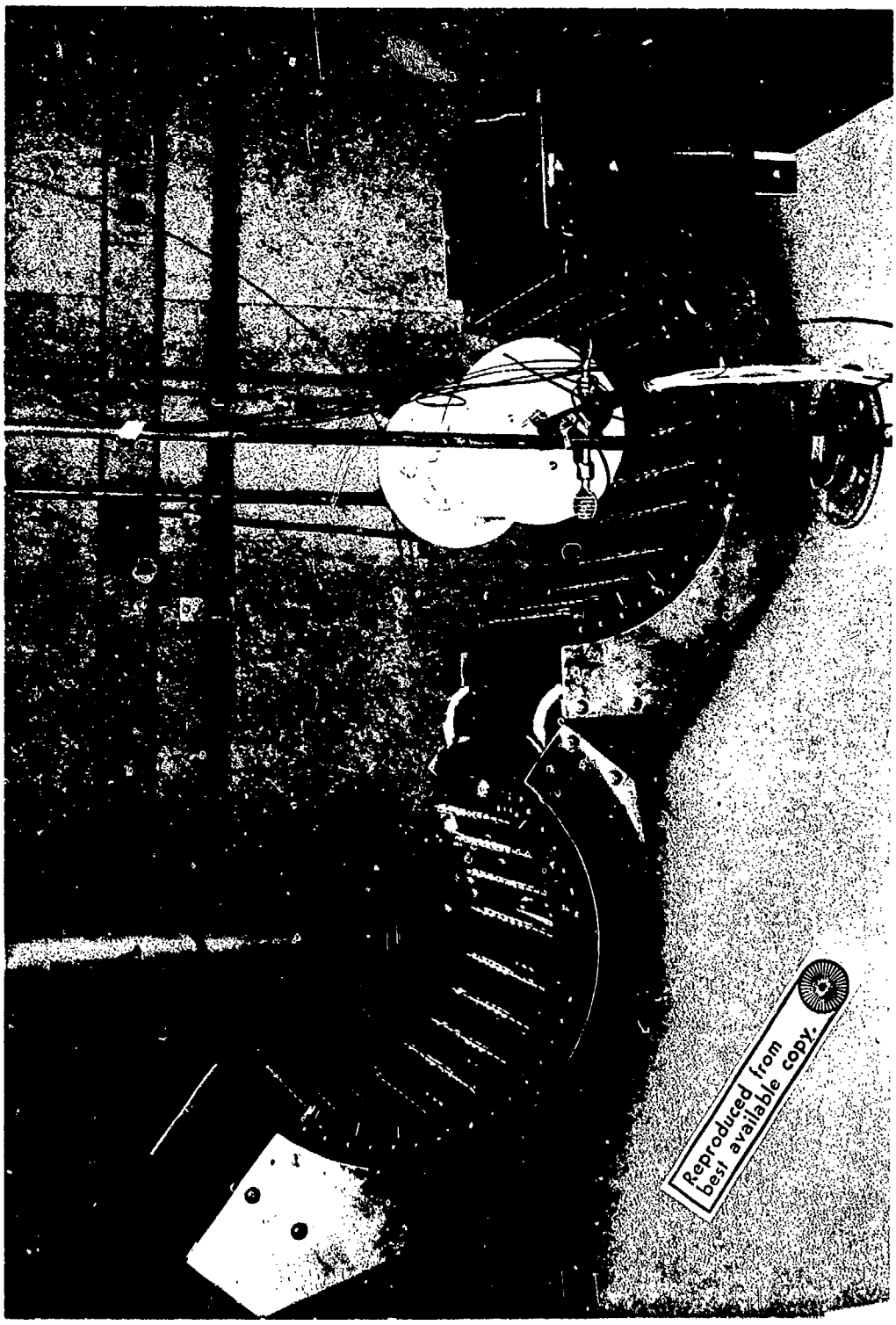

Fig. 1 ALUMINA A-SANDWICH CYLINDER IN CLAMSHELL HEATING FIXTURE

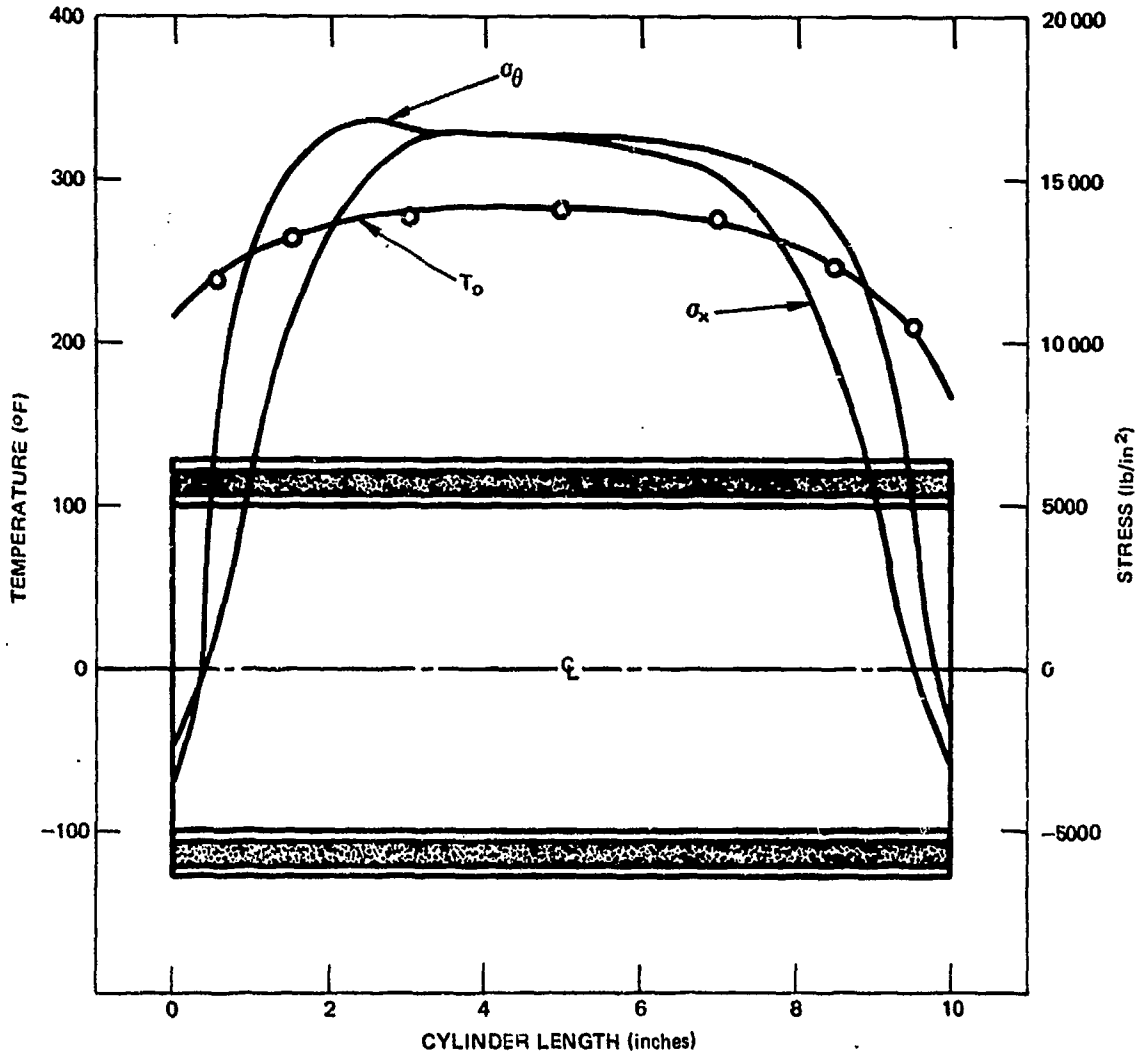

Fig. 2 MEASURED AXIAL SURFACE TEMPERATURES AND THEORETICAL STRESSES CONSIDERING AN AXIAL TEMPERATURE GRADIENT

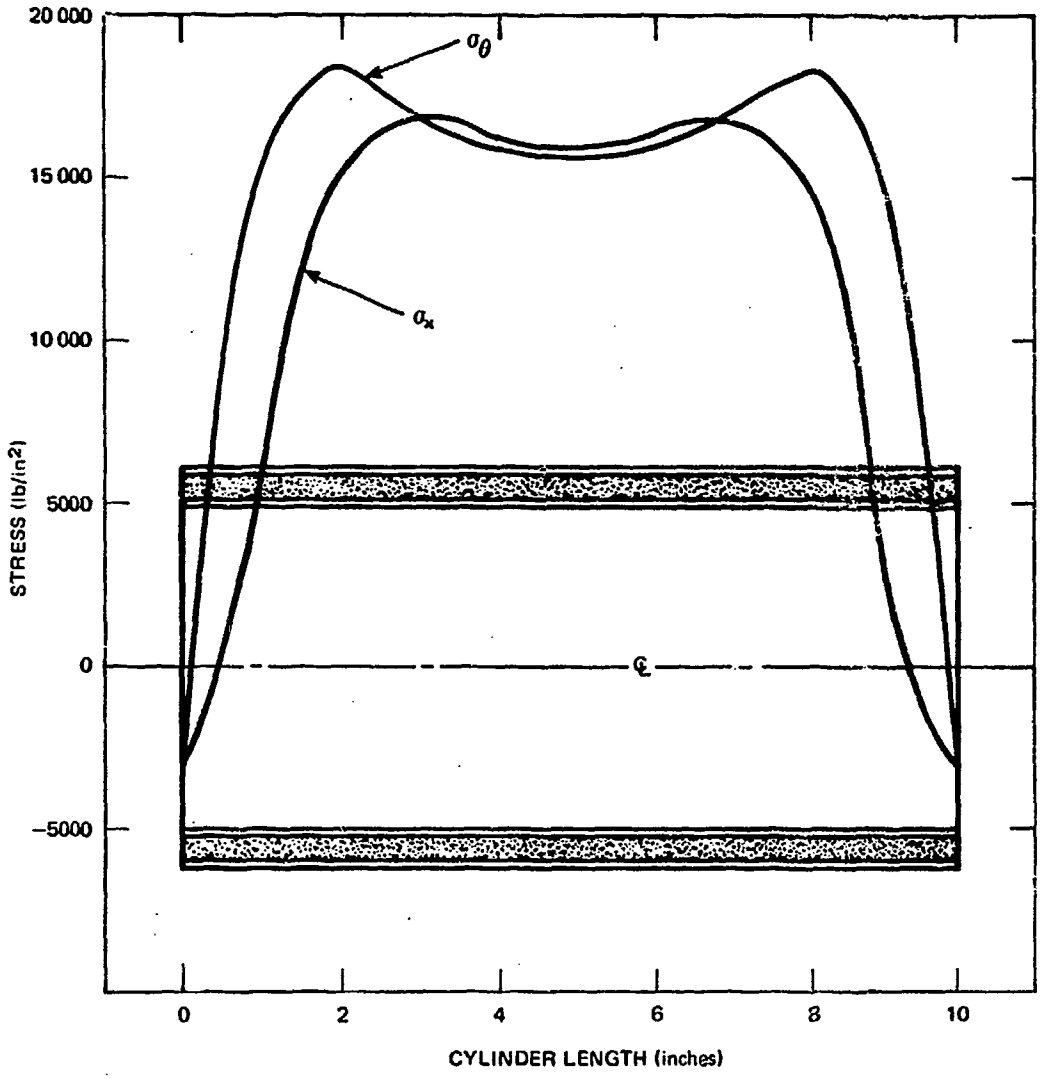

Fig. 3 THEORETICAL STRESSES COMPUTED ASSUMING NO AXIAL TEMPERATURE VARIATION

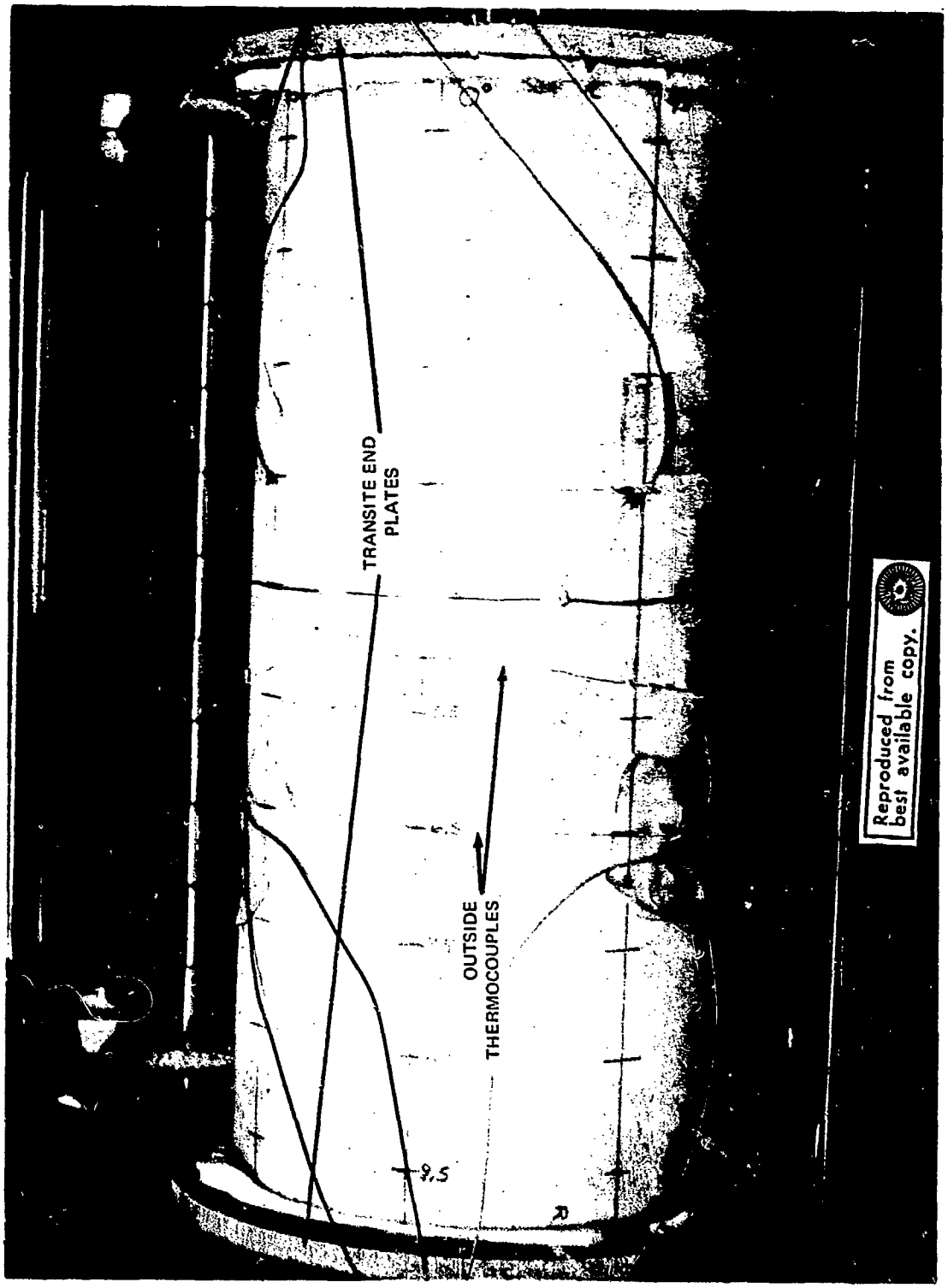

Fig. 4 ALUMINA CYLINDER IN HEATING FIXTURE

cylinders was done to eliminate undefinable heating to the inner surface.

For the first test of cylinder number 1, the outside temperature was increased to approximately 200°F in 30 seconds. It was anticipated that this would induce a moderate thermal stress level, and that subsequent runs would reach higher levels. Unexpectedly, at about 25 seconds into the run, a small but definite discontinuity in the stress record occurred. This discontinuity suggested that a small localized failure had occurred, relieving the stresses on the inside surface. Two more runs were made on this cylinder, and each helped to confirm that some failure had occurred in run 1. For the third test of cylinder number 1, a slightly higher heat flux was applied, and at about 30 seconds into the run an audible cracking occurred and the strain records indicated a sizable jump. At the time of this failure the strain gages indicated a stress level of approximately 13 000 psi. However, this level may have been influenced by the partial failure (most likely in the core) belived to have occurred in run number 1. Figure 5 is a photograph showing the internal surface of the cylinder after it was dye-checked. The dye has made the cracks readily visible, and has also caused the discororations on the end of the cylinder.

The second cylinder was instrumented and tested initially at substantially lower heat fluxes because of the experience with the first cylinder. As a result of this care, eight runs were made over a range of heat fluxes with excellent results. In run number 12, the heat flux caused thermal stress failure much like that observed in run number 3 of the first cylinder. The stress level recorded at the time of failure was approximately 15 000 psi, which is in close agreement with the failure level recorded for cylinder number 1. At this point it is important to emphasize the extremely low heat flux levels that were imposed upon these two test cylinders. The following paragraphs present a detailed discription of the temperature histories applied, the stresses recorded, and a discussion of the correlation results.

Fig. 5 CRACK PATTERN OF CYLINDER NUMBER 1 AFTER FAILURE

The first step toward a theoretical correlation of thermal stresses is the definition of the thermal gradient through the wall of the cylinders. A heat transfer program developed by APL (Ref. 6) was used for this purpose. The conductivity of the core material was evaluated with the following technique. Analytical models of the cylinders (Fig. 6) were devised and the measured outer surface temperatures were imposed on the model. The core conductivity was taken to be some constant percentage of the dense alumina conductivity reported in Ref. 10. This proportionality constant was varied until the theoretically calculated inner wall temperatures agreed with the measured inner wall temperatures. For cylinder number 1, this value was 6.74% of the dense conductivity.

Figure 7 shows the measured stresses and temperatures for run 1 of cylinder number 1. Also shown are the calculated temperatures and the predicted stress history from Rivello's theory. The measured and theoretical stresses agree to better than 20% at the worst point. This deviation can partly be explained from later observations of wall thickness variations along the circumference. As mentioned earlier, cylinder number 1 cracked on run 1, and for this reason no further theoretical correlations were attempted with this cylinder.

Figure 8 shows the results obtained for run 9 conducted on cylinder number 2. Here, two theoretical results of inside surface stress and temperature are presented to indicate the influence thermal conductivity variations have on the theoretical stresses. With the higher thermal conductivity (9% of the skin conductivity), the inside predicted temperatures are a maximum of approximately 5°F above the measured values; using a thermal conductivity of 6.74% of the skin conductivity, the maximum temperature difference is 6°F below the experimental values. Because these results are nearly bisected by the experimental data, it is expected that the best theoretical stresses also lie between these results. For at least part of the stress history, the experimental data fall between the two theoretical predictions. These test results indicate that a good correlation of the experimental results with theory was achieved.

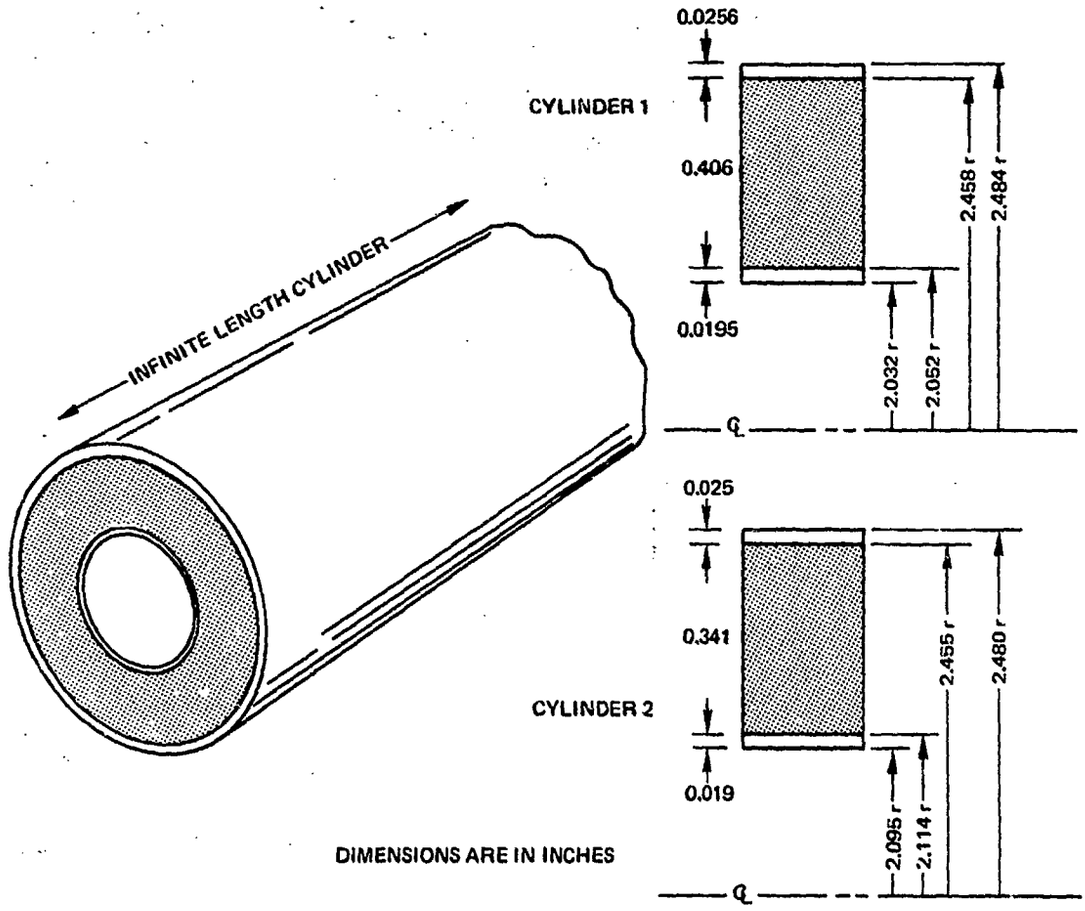

Fig. 6 ANALYTICAL MODELS FOR TEMPERATURE AND STRESS STUDIES

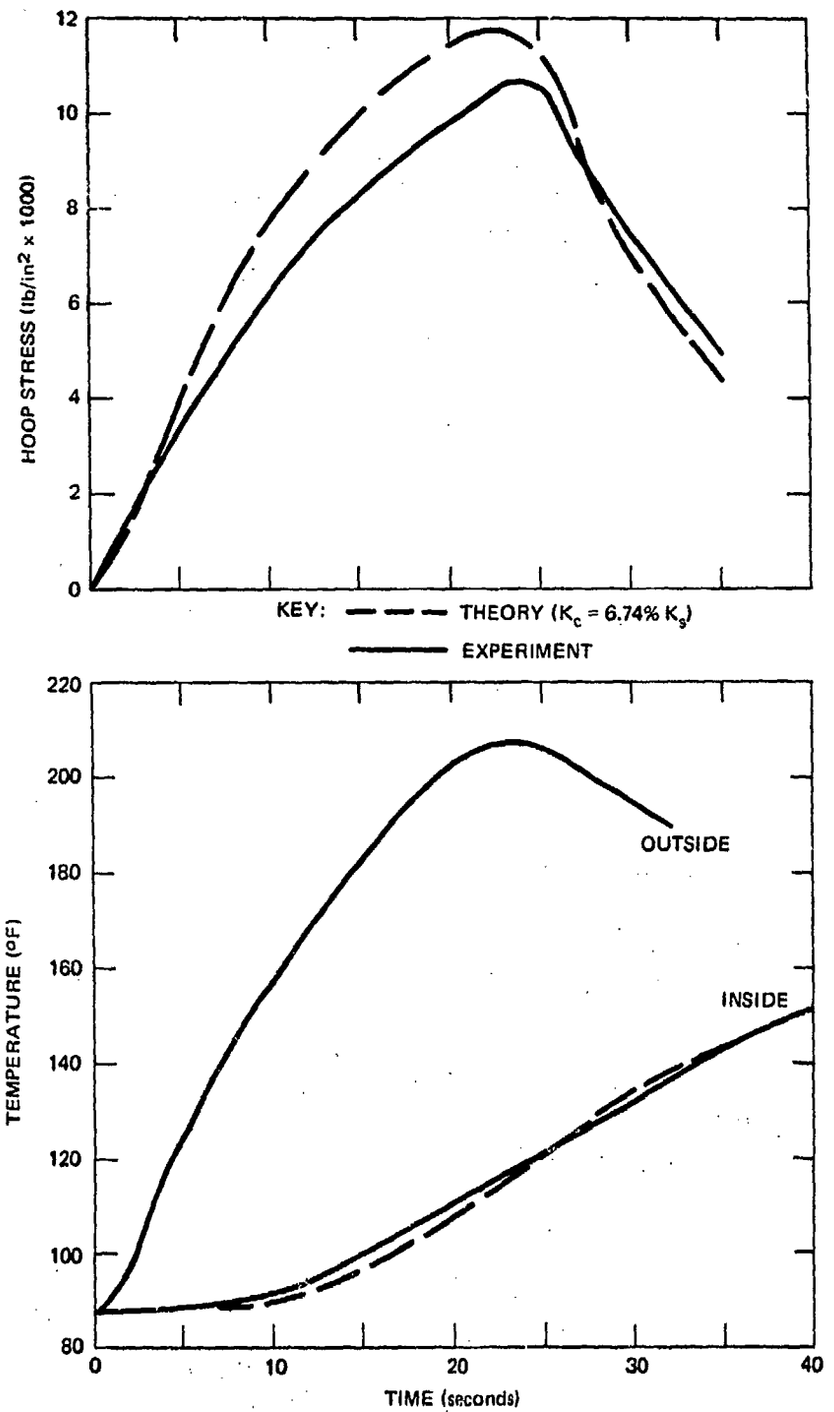

Fig. 7 ALUMINA A-SANDWICH TEMPERATURE AND STRESS CORRELATION FOR CYLINDER NUMBER 1, RUN 1

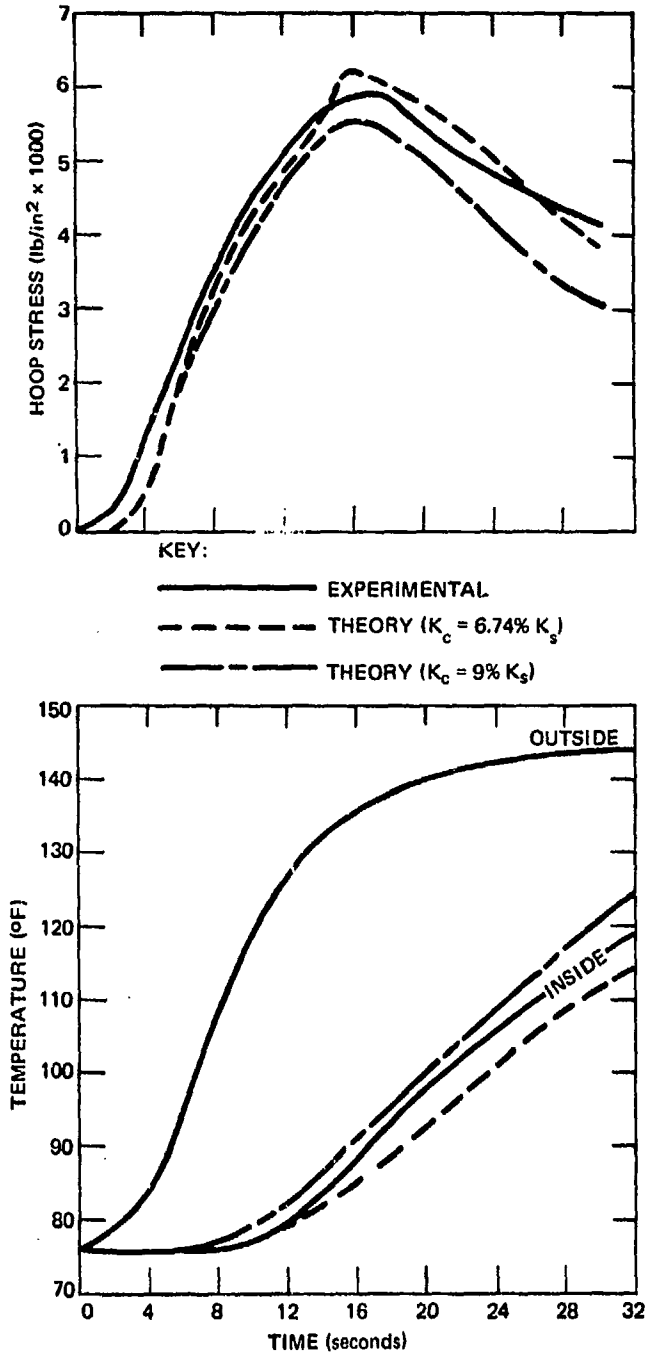

Fig. 8 ALUMINA A-SANDWICH TEMPERATURE AND STRESS CORRELATION FOR CYLINDER NUMBER 2, RUN 9

The results obtained for runs 11 and 12 are presented in Figs. 9 and 10, respectively. These particular runs were chosen for correlation study because they were the best test runs from the second cylinder test series. On several of the test runs there were false starts in which heating of the cylinder failed to follow the desired history. When this occurred, the test was aborted. The stress history of run 12 is presented (Fig. 10), with the time of stress failure in the specimen noted. This figure also shows the variation of experiment from theory, which appears to be larger than in runs 9 and 11. Possibly some stress failure had occurred previously between the skin and core, which would cause the experimental and theoretical stresses to diverge. Even so, the maximum variation of these deviations was less than 20%, as found in cylinder number 1. Combining the results presented in Figs. 8, 9, and 10, the percent error histories were calculated for the three runs. Results of this calculation are summarized in Fig. 11, which shows the maximum error is about 16% of the experimental data. This accuracy is quite good, considering the large number of variables involved in the test program.

As a result of the work presented in this section and the results of Figs. 7 through 11, the theoretical method developed and reported in Ref. 5 may be considered sufficiently accurate for predicting thermal stresses in alumina A-sandwich cylinders. Even though the experimental procedures used during the tests were considered satisfactory, it is suspected that the theoretical model deviated from the experimental test articles sufficiently to cause the variations that were noted in the correlation study. It is believed from the definitive information on the mechanical and thermal properties of the A-sandwich material, that the theoretical method (Ref. 5) used in this study for determining thermal stresses is adequate and would be in error by less than 20%. As stated previously, application of a cylindrical theory to evaluate radome stresses involves some amount of error depending on the proximity of the analysis to the tip region. Since the percent errors in the present correlation are attributable to measurement errors and test specimen uncertainties it is felt that the infinite cylinder theory of

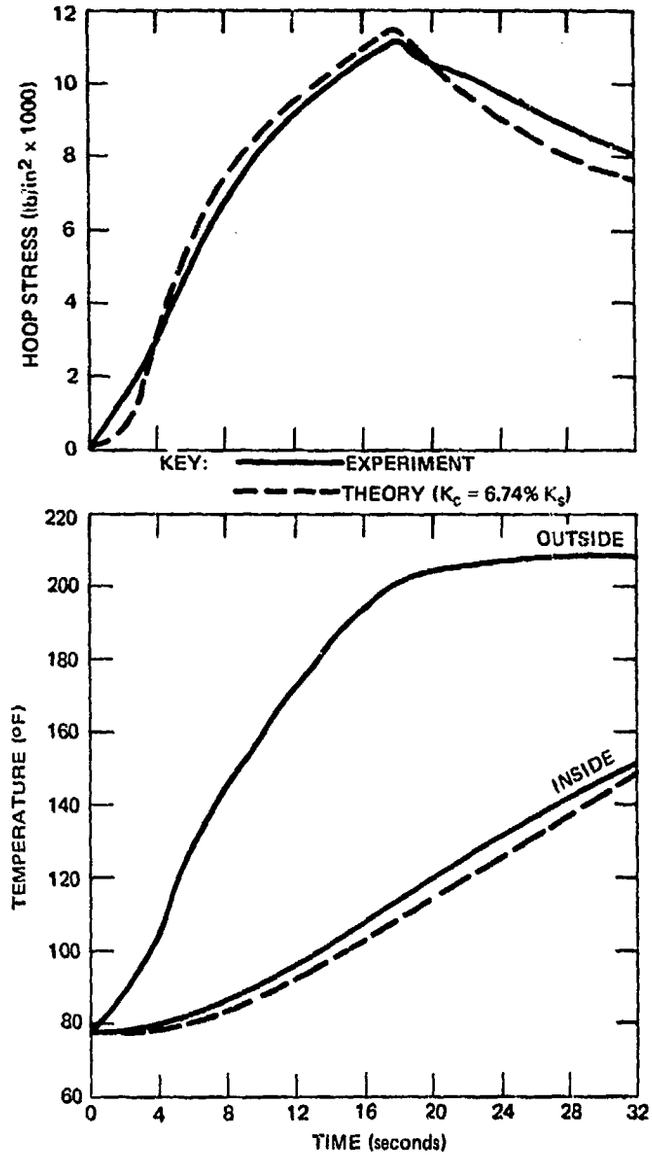

Fig. 9 ALUMINA A-SANDWICH TEMPERATURE AND STRESS CORRELATION FOR CYLINDER NUMBER 2, RUN 11

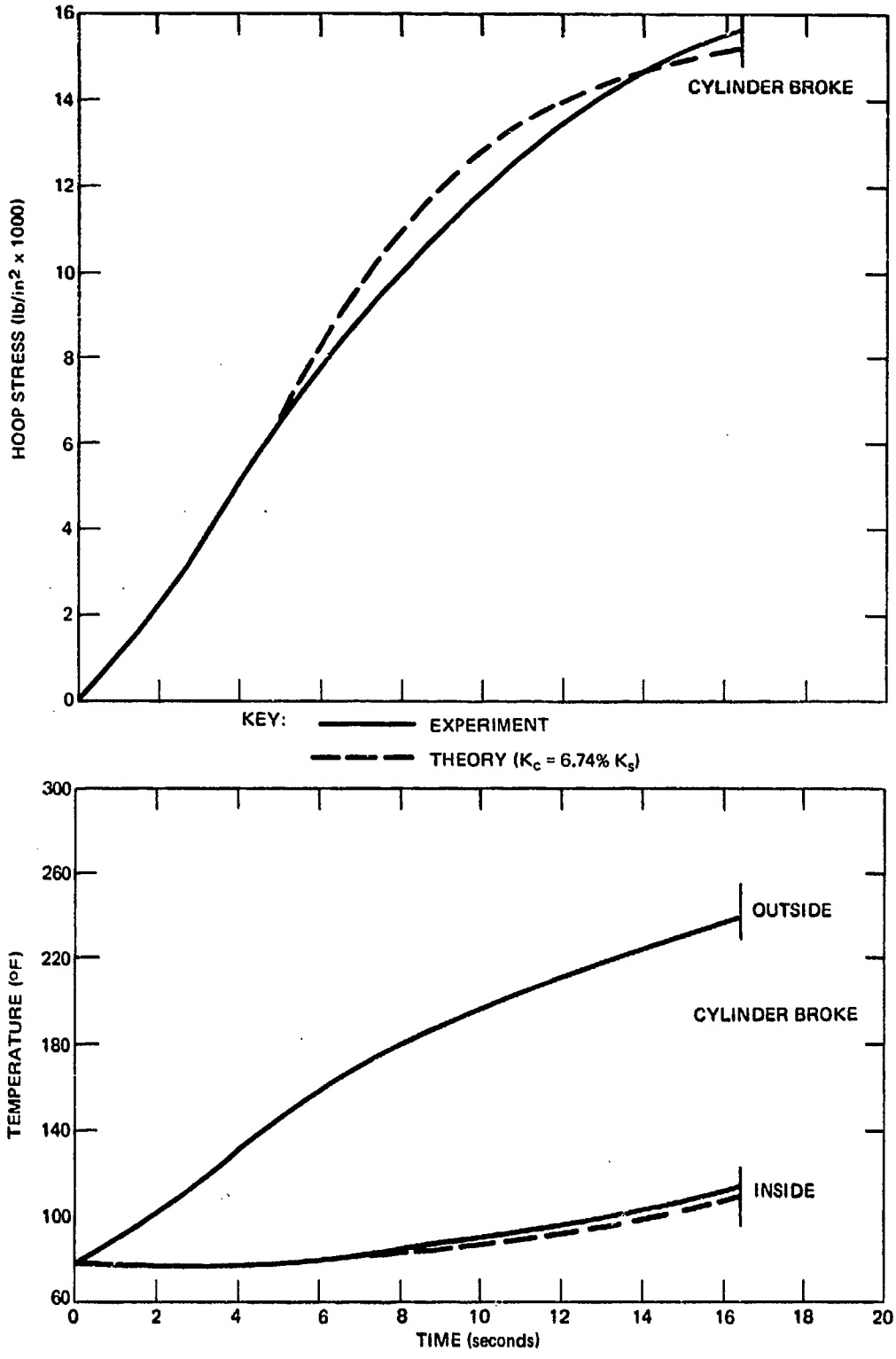

Fig. 10 ALUMINA A-SANDWICH TEMPERATURE AND STRESS CORRELATION FOR CYLINDER NUMBER 2, RUN 12

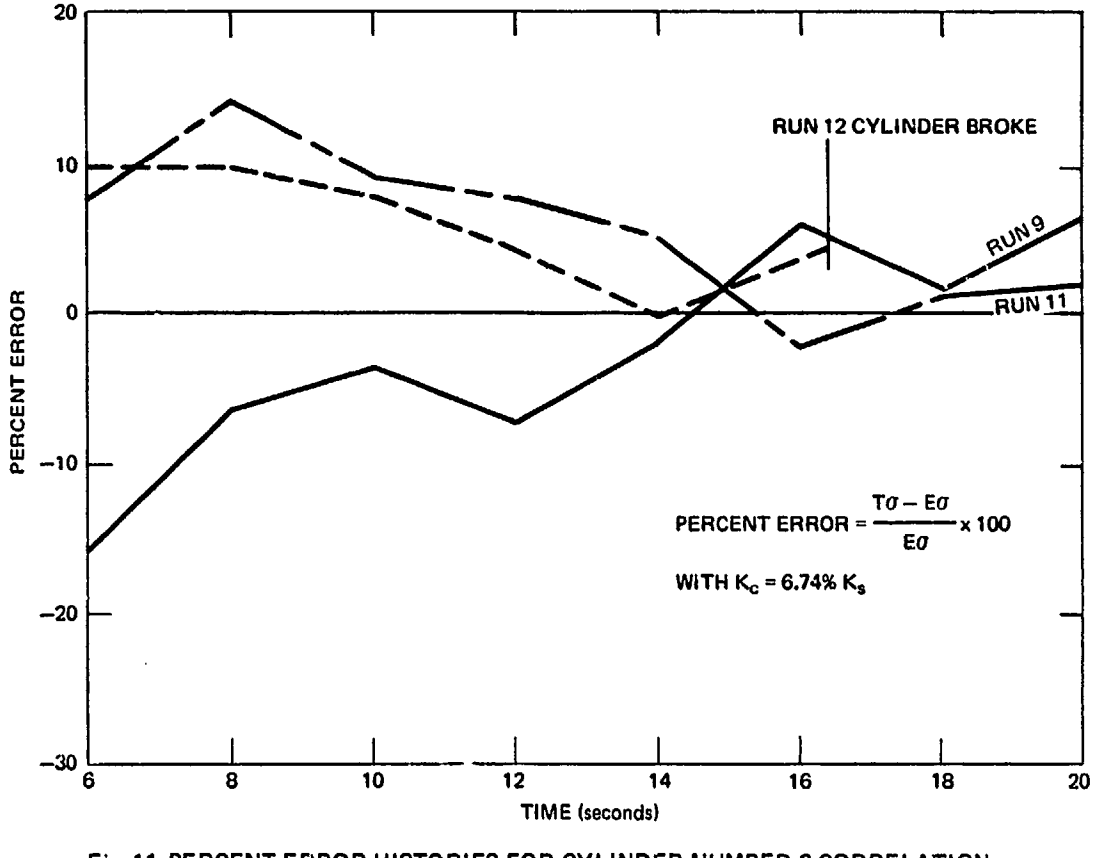

Fig. 11 PERCENT ERROR HISTORIES FOR CYLINDER NUMBER 2 CORRELATION

Rivello is adequate for making parametric studies and providing indicators as to the thermal stress efficiency of various sandwich (or monolithic) wall radome constructions.

4. POROSITY STUDIES

In designing monolithic radome structures the radome designer has only two basic wall thicknesses to choose from once the radar frequency and antenna geometry have been established. One is the half-wavelength wall, and the other is the "thin skin" wall considerably less than a half-wave thick. For ceramic materials, the thin skin is too weak to be practical and the half-wave wall is usually chosen. When an A-sandwich design is considered, there is no longer only a single choice for the design of a half-wave wall. A great variety of skin thicknesses and core porosities may be selected which will be suitable electrically. In attempting to define the flight limitations due to thermal stress of A-sandwich ceramic radomes, efficient use of time would suggest that an optimization study be made to find what combination of skin thickness and core porosity will provide the best resistance to thermal stresses. In order to accomplish such a parametric study, two essential relationships must first be defined: (a) an equation that shows which skin to core thickness ratios provide optimum transmission and (b) a relationship between porosity and the physical properties of the wall material. Reference 11 reports the following equation for relating skin thickness to core thickness with several other quantities as parameters:

$$d_c = \frac{\lambda}{2\pi\sqrt{\epsilon_c - \sin^2\theta}}\left[n\pi - \tan^{-1}\left(\frac{-r_s\,(1+r_{sc}^2)\sin 2\Phi_s}{-r_{sc}\,(1+r_s^2)+r_s\,(1+r_{sc}^2)\cos^2 2\Phi_s}\right)\right], \qquad (1)$$

where

$$2\Phi_s = \frac{4\pi d_s}{\lambda}\sqrt{\epsilon_s - \sin^2\theta}$$

Preceding page blank

d_c, d_s = core and skin thickness, respectively

θ = angle of incidence of the radar beam to the A-sandwich wall

λ = the wavelength in free space of the incident radar, which may be of parallel or perpendicular polarization

ϵ_s = dielectric constant for skin material

ϵ_c = dielectric constant for core material

r_s = skin to air reflection coefficient, a function of ϵ_s

r_{sc} = skin to core reflection coefficient, a function of ϵ_s, and ϵ_c

n = the "order" of the wall definition (n = 1 for 1/2 wavelength).

Solutions to this equation were generated by a computer program for alumina with 66% and 80% porous cores, and a plot of some of these solutions is shown in Fig. 12. The values of the other parameters are called out in the figure. The periodicity of the function is a result of the arc-tangent function. Also shown on the figure are the half-wave thicknesses for a dense monolithic wall at the four radar frequencies in S-, C-, X-, and K-bands. Note that the plane determined by the d_c and d_s axes (Fig. 12) identifies every possible symmetric A-sandwich wall design. The lines plotted on this plane represent the only designs which can be considered, because only these designs allow optimum radar transmission efficiency at the specified wavelength.

As noted previously, the current study includes examining the effects of varying the skin thickness and the core porosity of electrically equivalent half-wave ceramic walls to discover what combination of skin thickness and core density produces the greatest resistance to thermal stress. In order to perform this parametric study, the

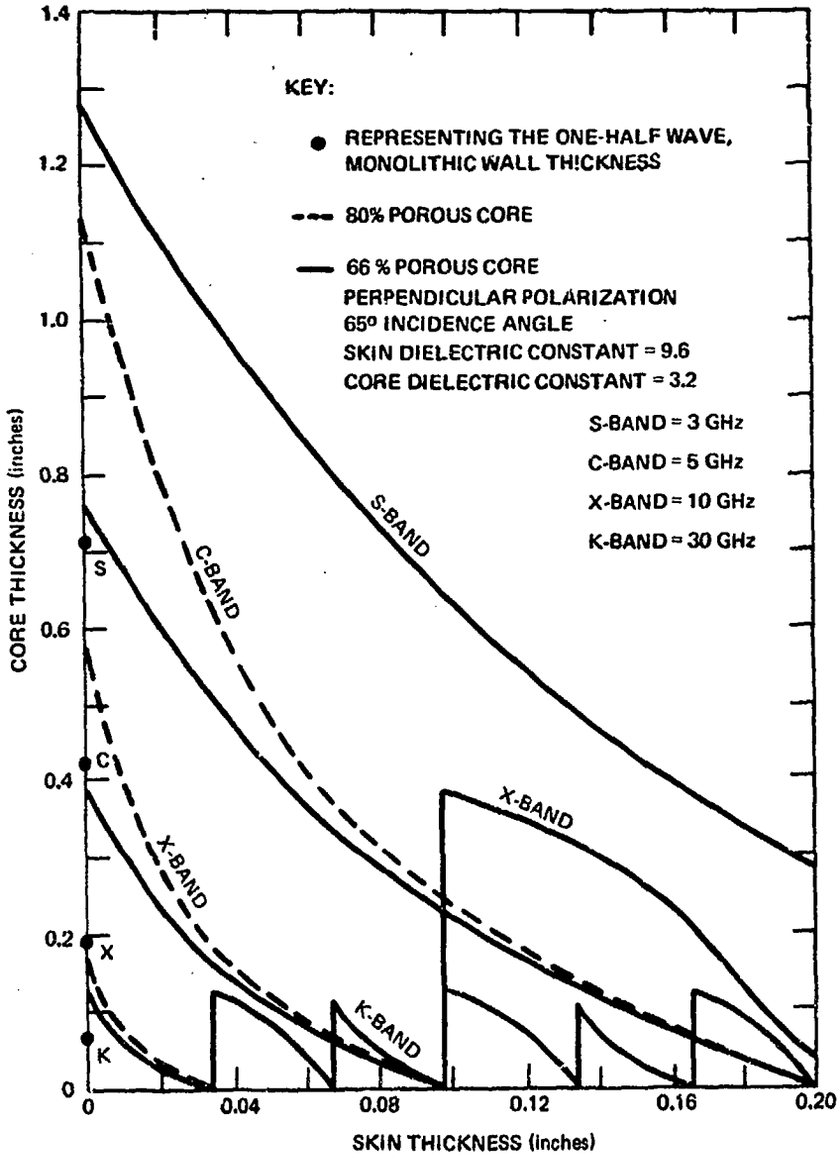

Fig. 12 CORE THICKNESS VERSUS SKIN THICKNESS FOR ALUMINA A-SANDWICH WALLS AT S-, C-, X-, AND K-BAND FREQUENCIES

effect of porosity on the thermal and mechanical properties of the ceramic must be known. A survey of the literature has revealed various experimental and theoretical treatments of this subject and the following discussion will attempt to compile this information as it applies to foamed slip cast alumina.

The physical properties of interest in a thermal stress study include density (ρ), specific heat (c_p), thermal conductivity (k), elastic modulus (E), Poisson's ratio (ν) and the coefficient of linear thermal expansion ($\bar{\alpha}$). In the current study, where it is of interest to calculate the effects on thermal stress of varying the core density in alumina A-sandwich and 2-ply walls, it is necessary to know the dependence of these properties on bulk porosity.

DENSITY AND SPECIFIC HEAT

The equation which will be used to determine the temperature gradients across the sandwich walls is the basic Fourier conduction equation, written in a finite difference form:

$$\dot{q} = \sum_{i=1}^{n} k_i A_i \frac{\Delta T_i}{\Delta x_i} = V \rho c_p \frac{\Delta T}{\Delta \tau}, \qquad (2)$$

where:

$\dot{q}$ = the time rate of heat flow into an element of volume, V

c_p = the specific heat of material

A_i = cross sectional area normal to the direction of heat flow between the volume and each adjacent volume

ΔT_i = the difference of temperature between V and adjacent volumes

Δx_i = the distance over which the temperature difference ΔT_i exists

ΔT = the change in temperature of the volume in the time interval $\Delta\tau$.

In this equation, the density-specific heat product (ρc_p) can be treated as a single constant, and it is this combined constant which will vary with porosity. As pores are introduced into a material, they displace a corresponding volume of dense material. Although the specific heat (c_p) of the pore material may be of the same magnitude as that of the solid material, the density of the pores is much less. Consequently, the total heat capacity (ρc_p) of the pore material may be neglected. With this assumption it is possible to say that the heat capacity of a porous material varies directly with the degree of porosity, i.e.,

$$(\rho c_p)_P = (\rho c_p)_d (1-P), \qquad (3)$$

where

P = is the volume fraction of pores, subscript P refers to the porous composite, and subscript d refers to the dense material.

POISSON'S RATIO AND COEFFICIENT OF THERMAL EXPANSION

Coble and Kingery (Ref. 12) report a study by Austin (Ref. 13) which shows that the porosity has no effect on the linear expansion coefficient. Kelly and Whatham (Ref. 14) report an investigation of the effect of porosity on Poisson's ratio in a ceramic material. They show that Poisson's ratio is also independent of porosity. It is therefore concluded that Poisson's ratio and the coefficient of expansion are independent of porosity.

THE ELASTIC MODULUS

In the search for a relation between Young's modulus and bulk porosity, considerable data for several types of alumina were found. References 15 and 16 present most of these data and propose the following empirical relation for describing the dependence:

$$E/E_o = e^{-bP}, \qquad (4)$$

where

- P = bulk porosity, as defined earlier
- E = modulus at porosity = P
- E_o = modulus at porosity = 0
- e = Naperian base
- b = empirical constant which best fits the particular data points.

Eight separate studies are presented in Refs. 15 and 16, all of which used different measuring techniques on samples of alumina which were fabricated by differing processes. These processes included hot pressing, cold pressing and slip casting. The measuring techniques included the resonant frequency technique, the velocity of sound technique, the transverse bend and flexural vibration techniques. Percent porosities ranged from 0.37% to about 50%. Figure 13 illustrates the significant observation which can be made from all these data: that the hot and cold pressed samples all fall along a fairly narrow band of values. The one set of slip cast data, which was measured by Coble and Kingery (Ref. 12), shows a markedly different trend.

The theory of Spriggs and Knudsen, (Eq. (4)) can be made to fit the data of Coble and Kingery if b = 2.73:

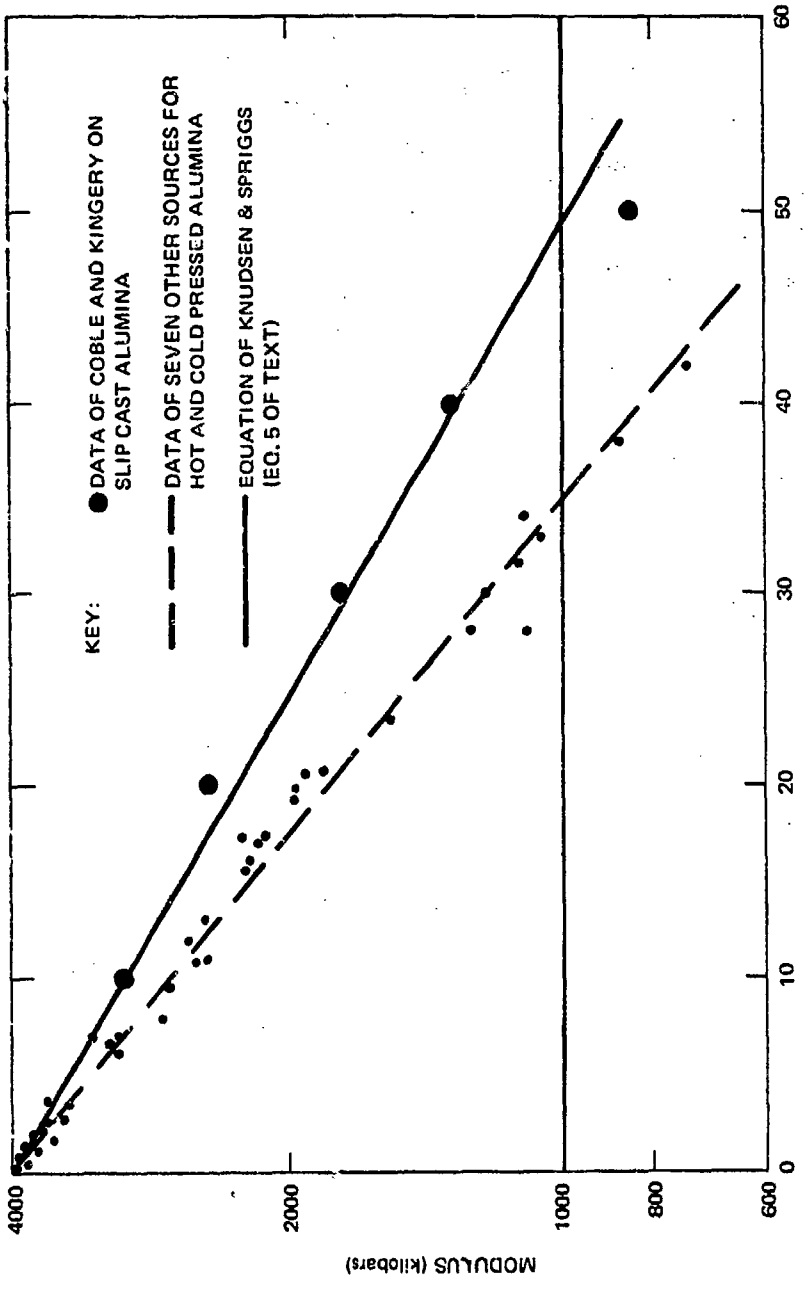

Fig. 13 YOUNG'S MODULUS VERSUS POROSITY FOR ALUMINA

$$E/E_o = e^{-2.73P} . \qquad (5)$$

Over the porosity range of 0 to 50%, Eq. (5) provides a good fit (Fig. 13); however, consideration of this equation will soon reveal that at a porosity near 100% (i.e., where the material is all pores) there is still a finite modulus indicated. Hasselman makes note of this fact (Ref. 17) and proposes an equation developed by Hashin (Ref. 18) of the form:

$$E/E_o = 1 + \frac{A'P}{1 - (A' + 1)P} , \qquad (6)$$

where

A' is an empirical constant and the other parameters are as defined earlier.

Hasselman uses the least squares technique to fit four of the eight sets of points reported by Knudsen and Spriggs to the above equation. Interestingly he chose only specimens which were cold or hot pressed and, specifically, he did not report on the slip cast specimens of Coble and Kingery. As a part of the present study, the five data points of Coble and Kingery were fit to Hasselman's equation and the fit was found to be overly sensitive to the 50% porous data point. As a result, the fit of Eq. (6) at low porosities is less precise than the fit at high porosities. Figure 14 shows the Hasselman equation (Eq. (6)) and the exponential fit (Eq. (5)) plus the experimental data. The other curve shown in Fig. 14 is discussed in the following paragraphs.

Coble and Kingery present what seems to be the best equation for fitting the data of the slip cast specimens. They use an equation derived by MacKenzie (Ref. 19):

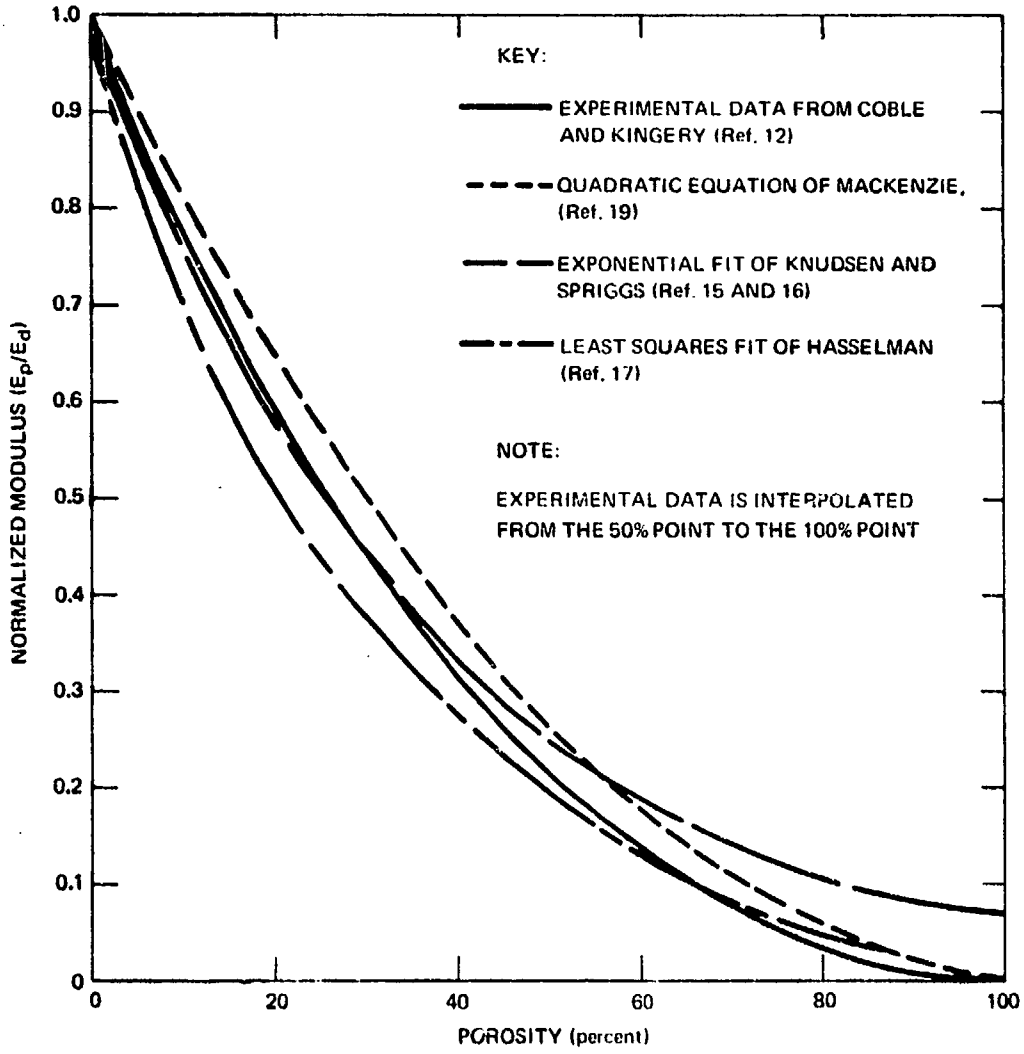

Fig. 14 NORMALIZED MODULUS VERSUS POROSITY FOR ALUMINA

$$1 - \frac{G}{G_o} = \frac{5(3K_o + 4G_o)}{(9K_o + 8G_o)} P + A'P^2, \qquad (7)$$

where

G = modulus of rigidity,

K = bulk modulus,

A' = constant value, and

subscript o refers to the properties of alumina in the dense (P = 0) state.

Using the identities:

$$K = \frac{E}{3(1-2\nu)} , \qquad (8)$$

and

$$G = \frac{E}{2(1+\nu)} , \qquad (9)$$

Eq. (7) can be rewritten in terms of Poisson's ratio:

$$E/E_o = 1 + \frac{15(\nu - 1)}{7-5\nu} P - A'P^2. \qquad (10)$$

The boundary condition of $E/E_o = 0$ at $P = 1$ yields:

$$A' = 1 + \frac{15(\nu - 1)}{7-5\nu} . \qquad (11)$$

Furthermore, for $\nu = 0.28$, which is a good average value for alumina and other ceramics, Eq. (11) becomes:

$$E/E_o = 1 - 1.92P + 0.93P^2. \qquad (12)$$

Figure 14 shows the data of Coble and Kingery along with the three "theoretical" fits described above, i.e., Knudsen and Spriggs (Eq. (5)), MacKenzie (Eq. (12)), and Hasselman (Eq. (6)). Up to about 50% porosity there would be little argument in using either the exponential (Eq. (5)) or the quadradic (Eq. (12)) expression. However, from 50% to 100% porosity the quadratic relation shows a closer correlation to the trend implied by the experimental data and will therefore be used for the current study.

THERMAL CONDUCTIVITY

McClelland and Petersen (Ref. 20) report on the variation of the room temperature value of thermal conductivity with porosity to values near 50%. The data was taken on hot pressed alumina whose density was varied by changing the sintering pressure and temperature. For porosities above 50% only a few references were found. An informal report by the Douglas Aircraft Co. reports on measurements of one sample at about 60% porosity. A paper by Pyron & Pears (Ref. 21) reports work with two samples of alumina, one at about 66% porosity the other at about 86%. The values of Porosity deduced from the cylinder tests of the first phase can also be used as a data point for a porosity of about 70%. All these data are plotted in Fig. 15 and they show a remarkable degree of consistency. The curve plotted in Fig. 15 is an empirical fit to the data points presented. Coble and Kingery make the observation that the thermal conductivity is the property which shows the largest sensitivity to the type of porosity introduced into a material. Materials which have continuous solid phases (i.e., the pores are voids introduced into the solid phase at the time of formation) show a moderate dependence of conductivity on porosity. In materials with a continuous pore phase (i.e. where the solid parts are small grains or spheres packed together such that only a minimal solid contact exists between grains) the conductivity varies sharply with porosity. To quote from Ref. 12, "For these different types of porosity the relative conductivity may differ by a factor of 5 to 10 at a constant amount of porosity". The

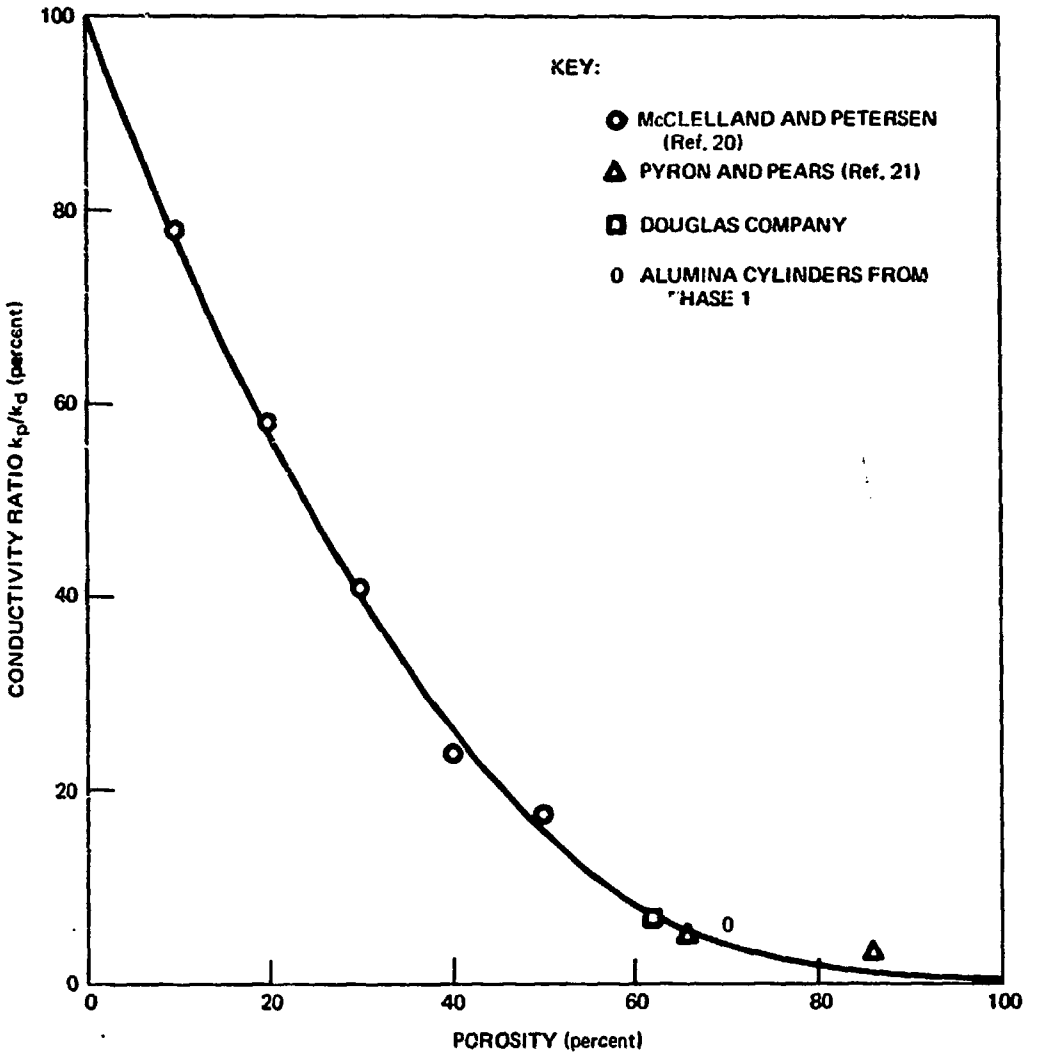

Fig. 15 THERMAL CONDUCTIVITY VERSUS POROSITY FOR ALUMINA

curve of Fig. 15 falls within a band of values reported by Coble and Kingery to be representative of intermediate types of porosity.

Introducing porosity into a material generally reduces the material's thermal conductivity. However, at elevated temperatures, radiation heat transfer across the pores tends to increase the apparent conductivity of the material. In an effort to discover the relative magnitude of such a mode of heat transfer in porous materials at high temperature, the following approximation of a pore was considered. The pore is assumed to be laminar; i.e., two parallel surfaces, one at temperature T_1 and the other at T_2 separated by a distance d:

Both surfaces have the same emissivity ϵ and absorptivity α. It is desired to know the net heat flux per unit area ($\dot{q}_{net}$) across the imaginary plane spaced between the two given planes. This flux will be the total radiated heat per unit area from the surface at T_1 less the heat radiated from the surface at T_2 plus a consideration for the energy reflected at each surface. In algebraic terms:

$$\dot{q}_{net} = (\epsilon\sigma T_1^4) - (\epsilon\sigma T_2^4) + (1-\alpha)\epsilon\sigma T_2^4 - (1-\alpha)\epsilon\sigma T_1^4 + (1-\alpha)^2\epsilon\sigma T_1^4 - (1-\alpha)^2\epsilon\sigma T_2^4 + \ldots \quad . \tag{13}$$

where

σ is the Stefan Boltzman constant.

The first two terms are the primary radiation terms, the third term represents the heat radiated by surface 2 but reflected at surface 1, the fourth term is the heat similarly reflected from surface 2, and the successive terms represent the continuing reflections that proceed indefinitely. Equation (13) can be simplified to:

$$\dot{q}_{net} = \epsilon\sigma \left[T_1^4 - T_2^4 + T_1^4 \sum_{n=1}^{\infty} (1-\alpha)^n (-1)^n - T_2^4 \sum_{n=1}^{\infty} (1-\alpha)^n (-1)^n \right], \tag{14}$$

or,

$$\dot{q}_{net} = \epsilon\sigma(T_1^4 - T_2^4) \sum_{n=0}^{\infty} (1-\alpha)^n (-1)^n . \tag{14a}$$

The infinite sum is equal to:

$$\sum_{n=0}^{\infty} (1-\alpha)^n (-1)^n = \frac{1}{2-\alpha} , \tag{15}$$

and if we assume that $\epsilon = \alpha$, and

$$T_1^4 - T_2^4 \approx 4\,\bar{T}^3 (T_1 - T_2),$$

then Eq. (14) becomes

$$\dot{q}_{net} = \frac{4\epsilon\sigma\bar{T}^3}{(2-\epsilon)} \quad (T_1 - T_2), \tag{16}$$

where

$\bar{T} = \frac{T_1 - T_2}{2}$, or the average temperature of the pore.

If we now consider the distance between the surfaces (d) and rewrite Eq. (16):

$$\dot{q}_{net} = \frac{4\epsilon\sigma\bar{T}^3 d}{(2-\epsilon)} \quad \frac{(T_1 - T_2)}{d}, \tag{16a}$$

then the term $\frac{4\epsilon\sigma\bar{T}^3 d}{(2-\epsilon)}$ can be regarded as the "effective" thermal conductivity of the space, d, between 1 and 2; i.e.:

$$\dot{q}_{net} = k_{eff} \frac{\Delta T}{d},$$

with

$$k_{eff} = \frac{4\epsilon\sigma\bar{T}^3 d}{(2-\epsilon)}. \tag{16b}$$

The above treatment is for laminar "pores" (i.e. parallel, infinite plates) but similar analyses can be done considering the geometrical differences for spherical pores. Such a study is contained in Ref. 22, and the geometrical differences can be reduced to one more term in the expression for k_{eff}:

$$k_{eff} = \frac{\gamma 4\epsilon\sigma\bar{T}^3 d}{(2-\epsilon)} , \qquad (17)$$

where:

γ = 1 for laminar pores and cylindrical pores with axes parallel to the heat flow,

$\gamma = \frac{2}{3}$ for spherical pores,

$\gamma = \frac{\pi}{4}$ for cylindrical pores with the axes perpendicular to the heat flow.

Several different equations of conductivity versus porosity and temperature are found in the literature, but the most straightforward treatment seems to be the best. That is, considering the conductivity of the porous material as the sum of the parts due to: (a) the solid, (b) the air in the pores, and (c) the "effective" conductivity of radiation. In other words, the conductivity as a function of temperature, $k_P(T)$ would be:

$$k_P(T) = \beta k_d(T) + (1-\beta) k_a(T) + \frac{4\epsilon\sigma T^3 d}{(2-\epsilon)} , \qquad (18)$$

where

β = the room temperature conductivity ratio, k_P/k_d, which is dependent on the porosity as shown in Fig. 15,

subscript a is a reference to the air or whatever material constitutes the pores,

and the other variables are as described earlier.

The only data available for comparison to the functional relationship shown in Eq. (18) is a group of questionable data points reported by Pyron & Pears in (Ref. 21). A Sample of their data is plotted in Fig. 16 along with the

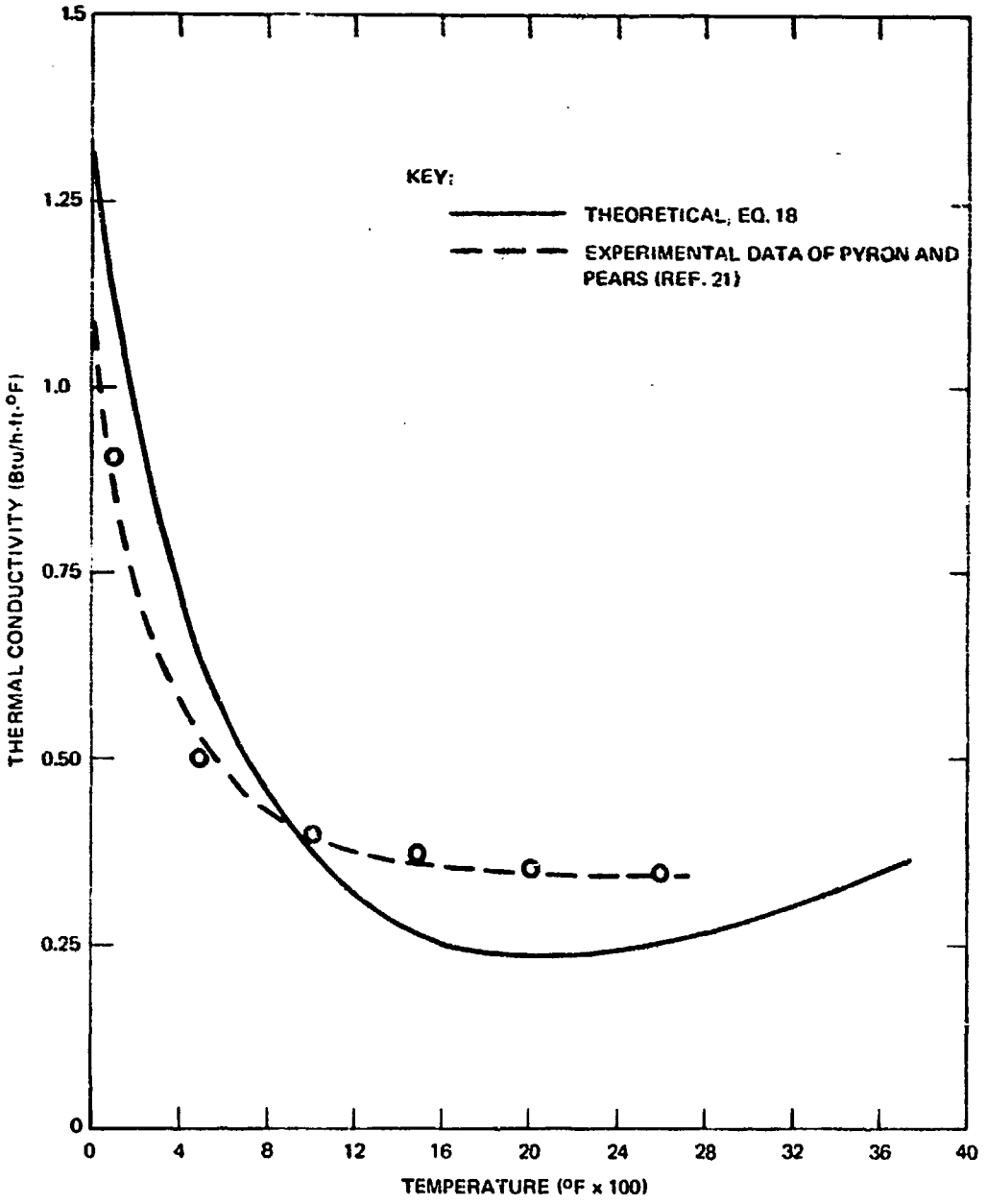

Fig. 16 THERMAL CONDUCTIVITY VERSUS TEMPERATURE FOR 66% POROUS ALUMINA

corresponding data from Eq. (18) using a porosity of 66% and a pore diameter of 0.01 inch. No significant conclusion can be made from the apparently good correlation shown in Fig. 16 because of uncertainities in the authenticity of the data. For example, the data was taken by two different techniques, one at room temperature and one at higher temperatures. Furthermore, the tests were run at a reduced pressure and there is no guarantee that the conductivity values used in Eq. (18) for the dense material would match those of Ref. 21.

In order to show what is implied by Eq. (18), Fig. 17 presents several plots of k_p versus T for differing porosities. Figure 18 shows a curve of k_p versus T for a high porosity sample and also shows variations cuased by changing the pore size (d). The expanded scale of Fig. 18 should be noted along with the observation that it takes a very large variation in pore diameter to affect significant changes in the effective conductivity at high temperatures.

With the above porosity functions defined, it was then possible to conduct the parametric study for optimizing the thermal stress resistance of A-sandwich radomes on supersonic trajectories. The following discussion will describe the analytical procedures used and the results which were obtained.

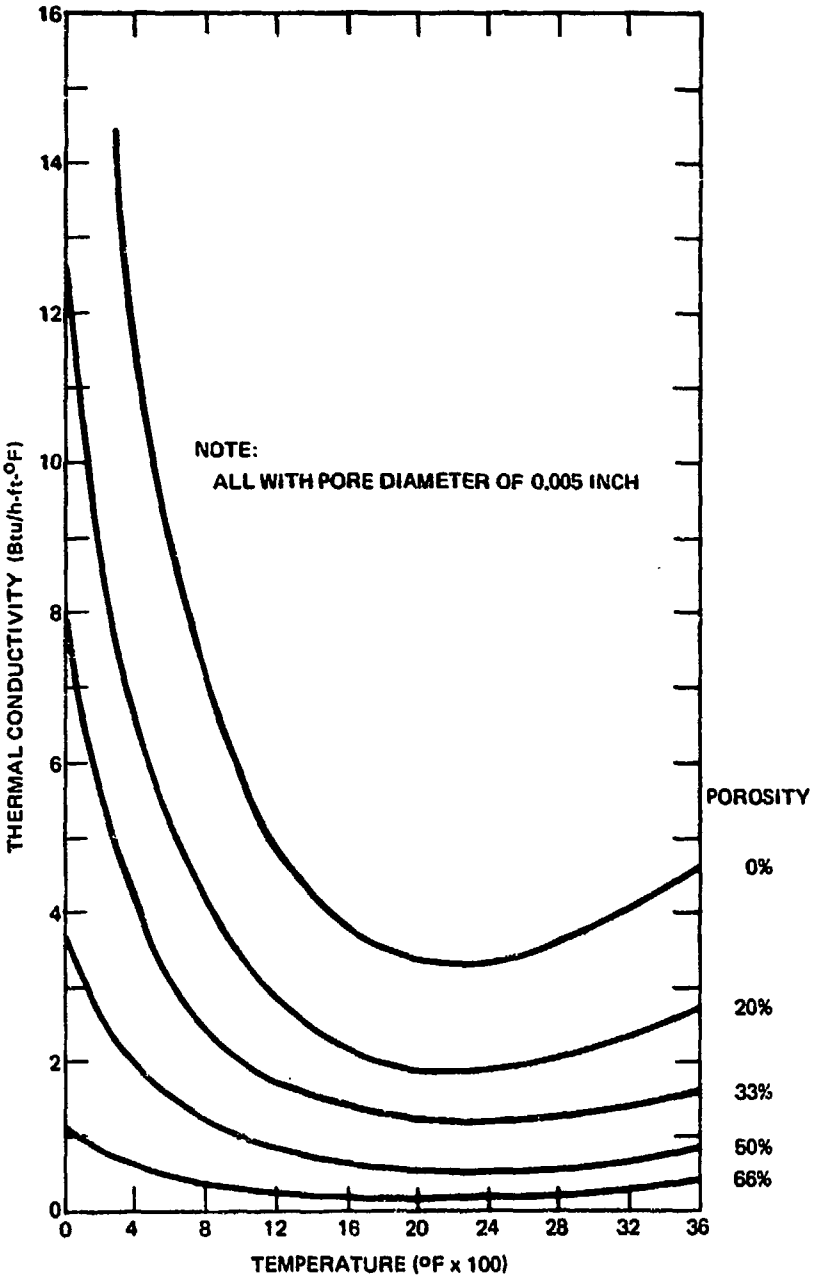

Fig. 17 THERMAL CONDUCTIVITY OF ALUMINA VERSUS TEMPERATURE FOR VARIOUS POROSITIES

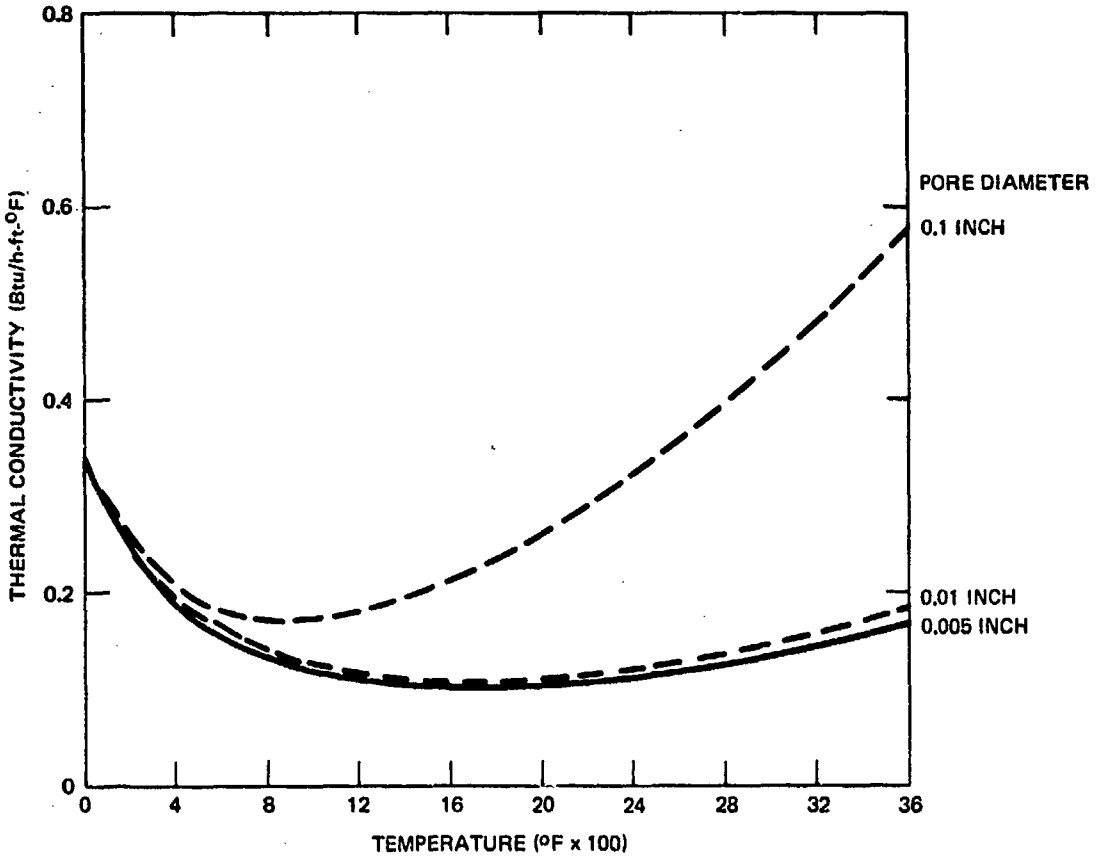

Fig. 18 THERMAL CONDUCTIVITY OF ALUMINA VERSUS TEMPERATURE AT 80% POROSITY FOR VARIOUS PORE DIAMETERS (NOTE EXPANDED CONDUCTIVITY SCALE)

5. LIMITATION STUDIES

THEORETICAL PROCEDURES

The aerodynamic heating of the A-sandwich walls is calculated using Eckert's reference enthalpy technique. The transient conduction and radiation heat transfer is calculated using a lumped mass, forward marching, finite difference computer program (Refs. 6 and 7) developed at APL (cf. Eq. (2)). Coupled with this heat transfer program is a subroutine which will compute thermal stresses according to the theory of Rivello. The radome shape which this analysis will simulate is a 28.3-inch-long Von Karman curve with a fineness ratio of 2.1. The maximum heating location for such a shape has been shown to occur where the flow changes from laminar to turbulent (Ref. 23). For this radome shape, the transition was assumed to occur 1.4 inches from the tip of the radome, measured along the surface. For the thermal stress calculations this location will be approximated by a cylinder with a radius measured normal from the surface to the centerline of the radome. Figure 19 shows a sketch of some of the analytical models used.

The flight environment considered for this study consisted of altitudes ranging up to 100 000 feet and velocities up to 12 000 ft/s. Specific trajectories were characterized by a launch angle (QE) and linear velocity history. The velocity histories used were annotated:

V1 for a constant acceleration of 266 ft/s^2

V2 for a constant acceleration of 400 ft/s^2

V2 for a constant acceleration of 600 ft/s^2

These velocity histories and launch angles cover the flight regimes of current as well as potential future missiles.

The first parameter studied which affects thermal stress resistance was skin thickness. Electrically opti-

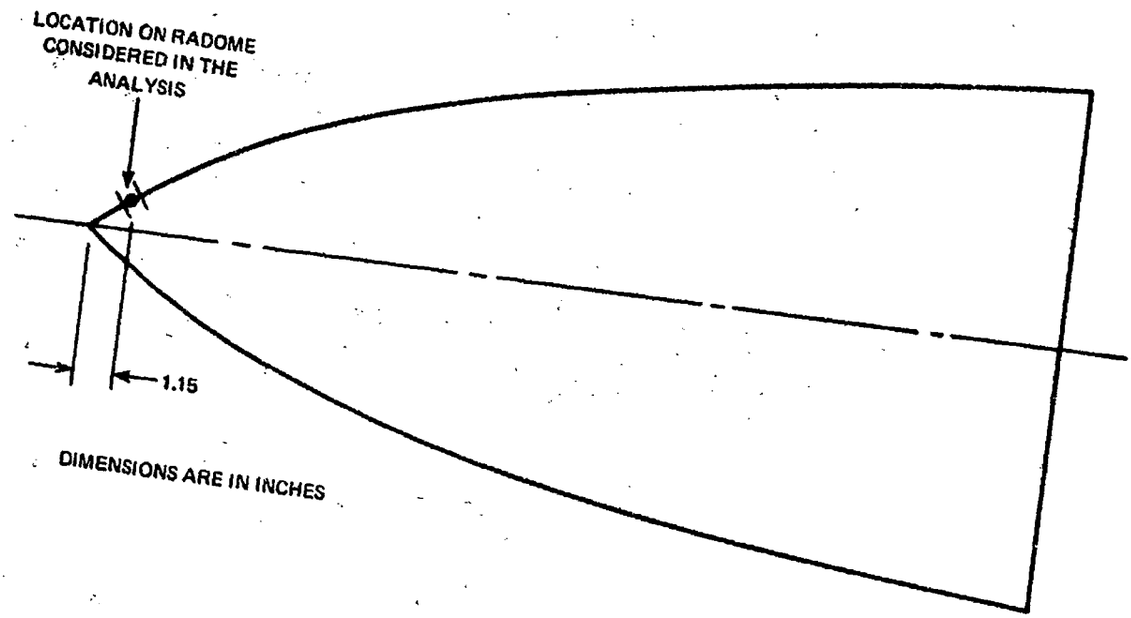

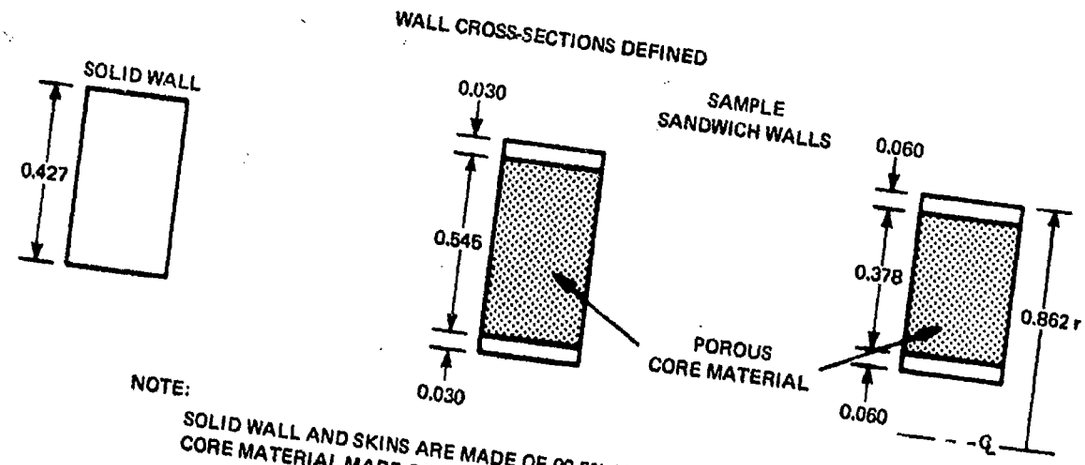

NOTE:
SOLID WALL AND SKINS ARE MADE OF 99.5% ALUMINA; DENSITY = 248 lb/ft^3;
CORE MATERIAL MADE OF 99.5% ALUMINA; 66% POROSITY

Fig. 19 DEFINITION OF RADOME AREA STUDIED FOR ALUMINA AT C-BAND

mized walls with several different skin thicknesses (all other parameters held constant) were flown on the same missile trajectory. The first cases studied were those of X-band alumina walls with core porosities of 66%. It should be noted that since the thickness of the monolithic alumna wall at X-band is approximately 0.20 inch, an A-sandwich with skins larger than 0.10 inch each will provide no weight advantage. Also, skins with thicknesses less than 0.005 inch are impractical from the point of view of handling as well as fabrication.

Figure 20 shows the stresses that were calculated at the inner wall for several sandwich walls with skin thicknesses in this interval. Inspection of the figure will show that there is no optimum skin thickness (i.e., no one design realizes lower stresses than others with either thinner or thicker skins. Furthermore, the monolithic wall realizes the lowest stresses and therefore is significantly better than any of the sandwich designs. It may also be noted that the A-sandwich design skin with 0.015-inch is the worst case; that is, skin thicknesses both larger and smaller than this value realize smaller stress histories. This is precisely the opposite of the optimum that was being sought.

The second design parameter studied was core porosity. In this case, for a given radar band the environment and skin thickness parameters were held constant while the core porosity was varied. Values of 50%, 66%, and 90% porosity were chosen because they represent the range of porosity considered practical from a weight savings as well as a fabrication and handling standpoint. Figure 21 shows the stress versus time data for three X-band radomes at V1, 80° QE and a skin thickness of 0.06 inch. Although the entire spectrum of core porosities was not studied, the figure shows a trend of better thermal stress resistance for decreasing porosity. It can be noted in Fig. 21 that the 66% and 80% porosity cases are very nearly the same. This can in part be explained by again noting Figs. 14 and 15; at 66% and 80% porosity the curves of conductivity and modulus are not greatly different. The

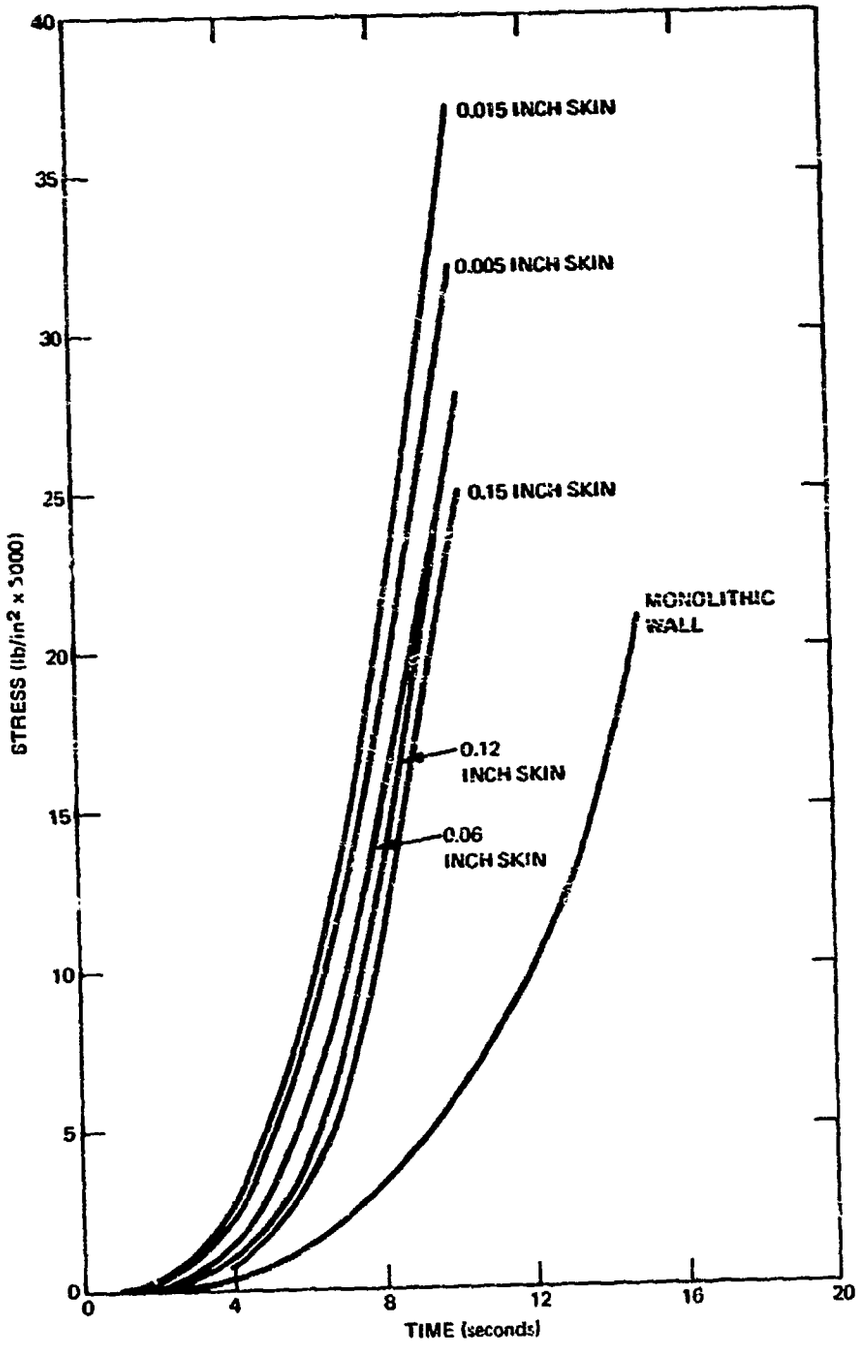

Fig. 20 MAXIMUM TENSILE STRESS VERSUS TIME FOR X-BAND ALUMINA WALLS, 66% POROUS CORE, V_1, QE = 80°

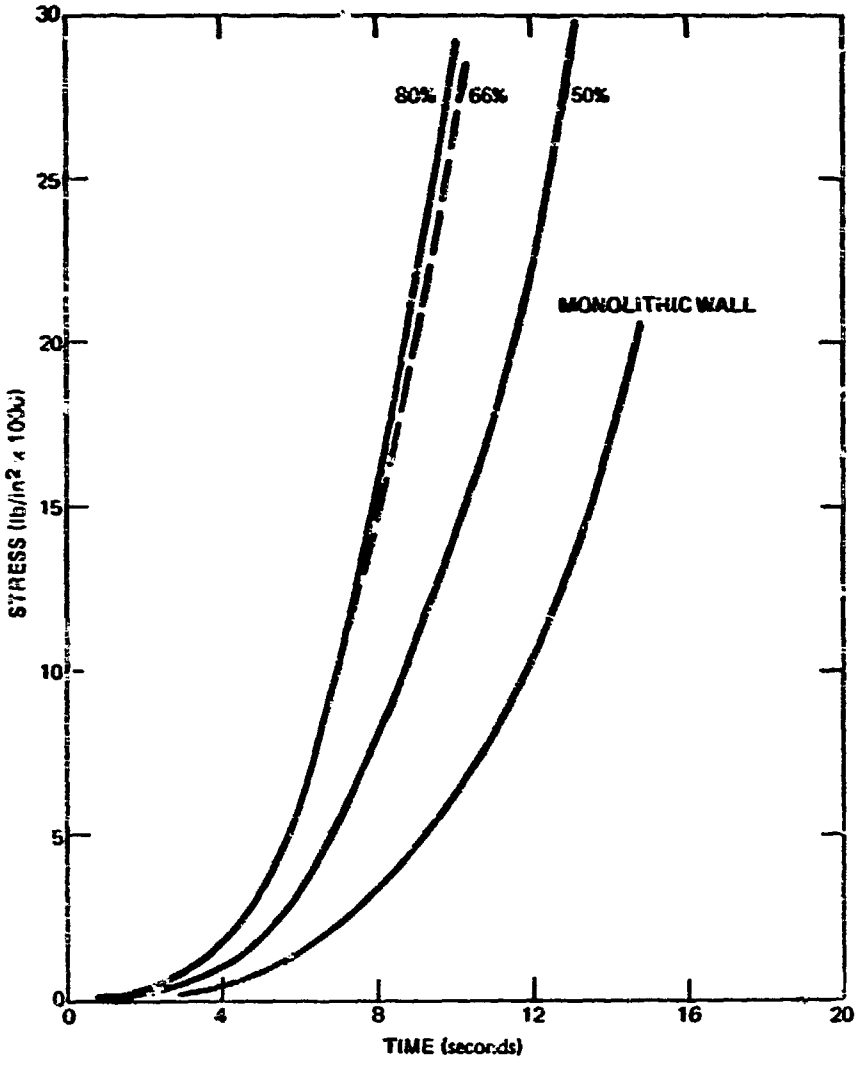

Fig. 21 TENSILE STRESSES FOR COMPARABLE ALUMINA X-BAND WALL DESIGNS AT CORE POROSITIES OF 50%, 66%, AND 80%, SKIN THICKNESS = 0.06 INCH, V1 VELOCITY HISTORY AT 80° QE

largest changes of these properties occur at the lower porosities. As a result of this, the modulus and conductivity at 66% porosity and 80% porosity are not greatly different.

The conclusion drawn from the data presented in Fig. 21 is similar to that for the skin thickness study: there is no core porosity which will realize a lower thermal stress than other porosities either larger or smaller. Moreover, the thermal stress optimization study has shown that there is no optimum A-sandwich design (i.e., no A-sandwich of skin thickness and core porosity realizes a minimum stress level in a given thermal environment). The consequence of this result is that several A-sandwich walls will have to be evaluated in the flight limitations study to gain an accurate description of the maximum A-sandwich flight capabilities.

FLIGHT LIMITS – ALUMINA

The flight limitations of a particular radome design due to thermal stresses are determined by calculating stresses in the design during several different trajectories. The time at which the stress history exceeds the design limit is then plotted in a velocity versus time coordinate system for several trajectories. The locus of these points defines an operating regime beyond which the missile cannot fly, under the assumption of linear acceleration. Other sources (Refs. 23 and 24) have reported calculation methods wherein the velocity history was allowed to vary in such a way that the limit stress was never exceeded. This velocity limit method produces a somewhat more complete thermal stress limit definition but is never higher than the limit reported here. Because of the complexity of this method it was not used on the many cases studied in this investigation.

Figure 22 presents thermal stress limits for 66% porous alumina A-sandwich radomes flown at an 80° QE for trajectories V1, V2, and V3. Skin thickness is shown as a

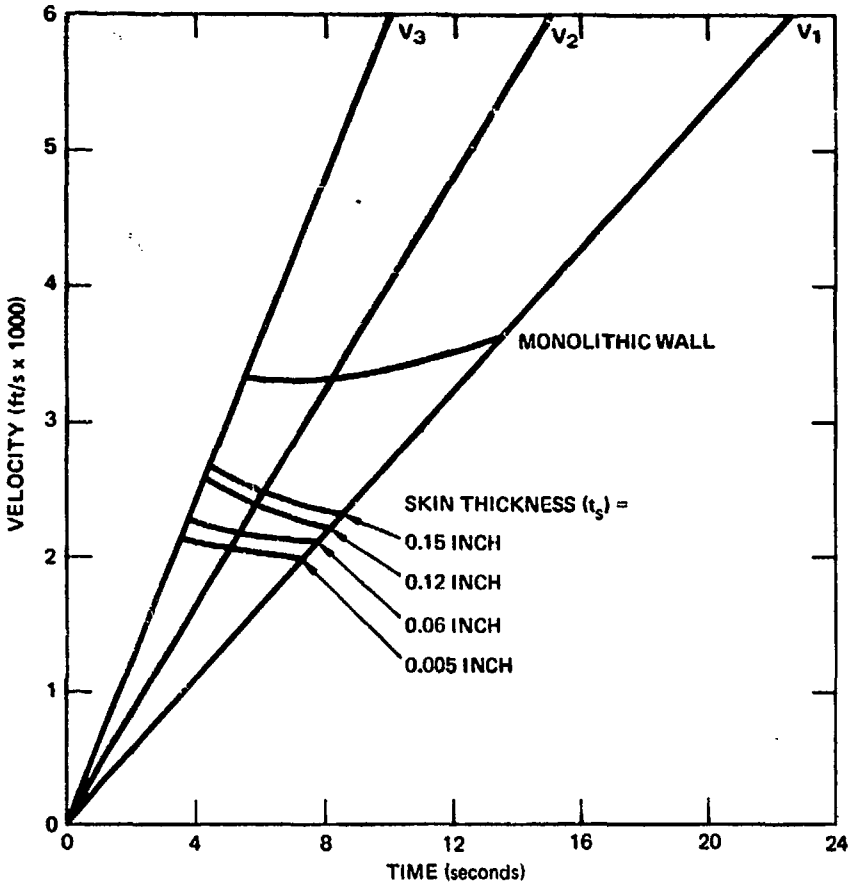

Fig. 22 VELOCITY LIMITS OF A-SANDWICH ALUMINA WITH 66% POROUS CORE AT X-BAND, $\theta E = 80^{o}$

parameter. Inspection of the figure shows all four sandwich designs limited to flights generally below Mach 3 and considerably below the monolithic wall limit, which is also plotted for comparison. Figure 23 presents data for two of the same walls at a QE of 20°, which represents the upper limit in thermal environment. An 80° launch angle achieves higher velocities at higher altitudes, while low launch angles achieve high velocities at low altitudes (where aerodynamic heating is more severe). Figure 23 shows the same basic trends as noted in Fig. 22, with all of the limits occurring at slightly earlier times. Figures 24 through 26 present similar data that were generated for alumina A-sandwich walls suitable for other radar frequencies. Figure 24 differs from the others in that the core porosity is 50% (the others are 66%). Comparing the data of Figs. 22 and 24 it may be noted that the low porosity core results in slightly higher limits.

It is evident from the above mentioned limit curves that the alumina A-sandwich design is severely limited by thermal stresses and that none of the cases studied showed performance better than the monolithic wall.

FLIGHT LIMITS – PYROCERAM 9606

After the limits results for alumina had been compiled and shown to be so low, it was decided to choose another material with significantly different physical properties and see if any different results would be obtained. Pyroceram 9606 was chosen because it exhibits properties different from alumina and because it is a currently used radome material. Correspondence with Corning Glass (the manufacturers of Pyroceram) revealed that no porous Pyroceram ceramic was yet being produced and no porosity dependent properties could be reported. In order to analyze a Pyroceram A-sandwich wall it was required to know the porosity dependence of the physical properties, so the data found for alumina was employed in the following way. The density and dielectric constant were taken as varying linearly with porosity. The expansion coefficient, Poisson's

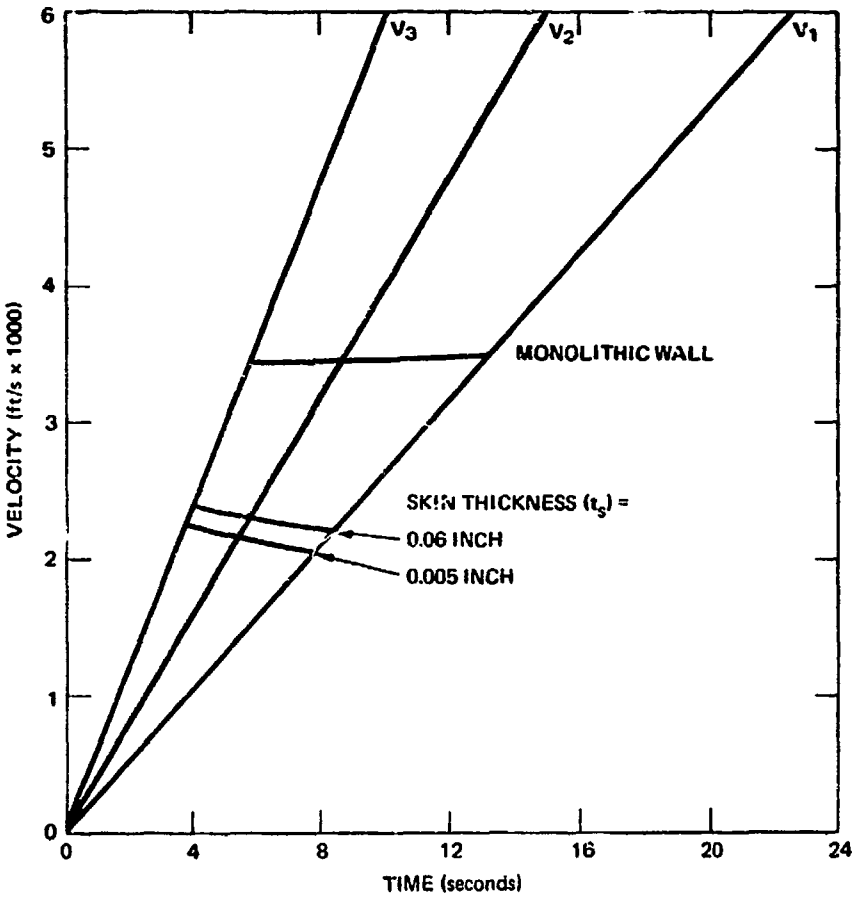

Fig. 23 LIMITATIONS OF ALUMINA A-SANDWICH AT 20° QE with 66% POROUS CORE, X-BAND

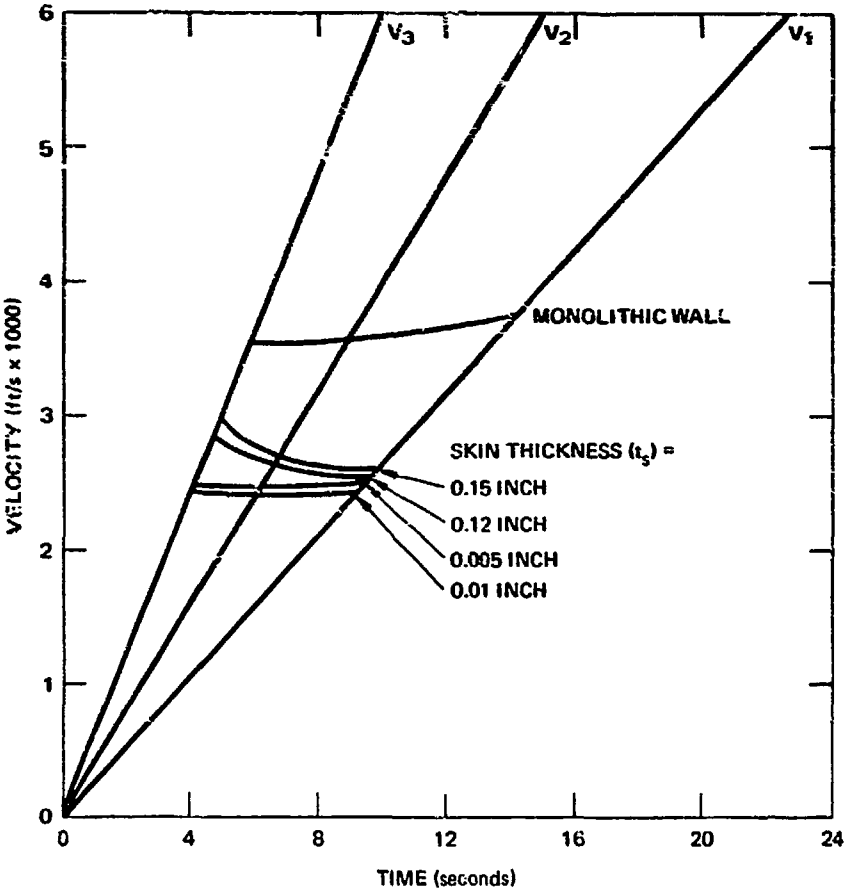

Fig. 24 LIMITATIONS OF ALUMINA AT 50% POROSITY, X-BAND RADAR, QE = 80°

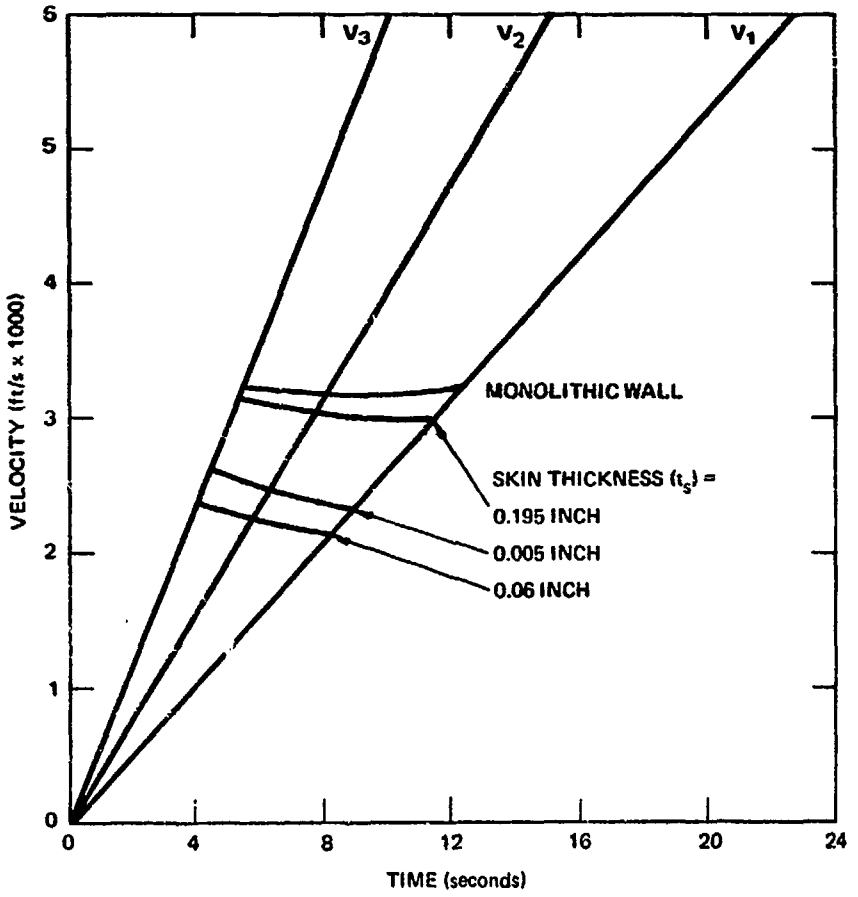

Fig. 25 LIMITATIONS OF ALUMINA A-SANDWICH WITH C-BAND RADAR, 66% POROSITY, 80° QE

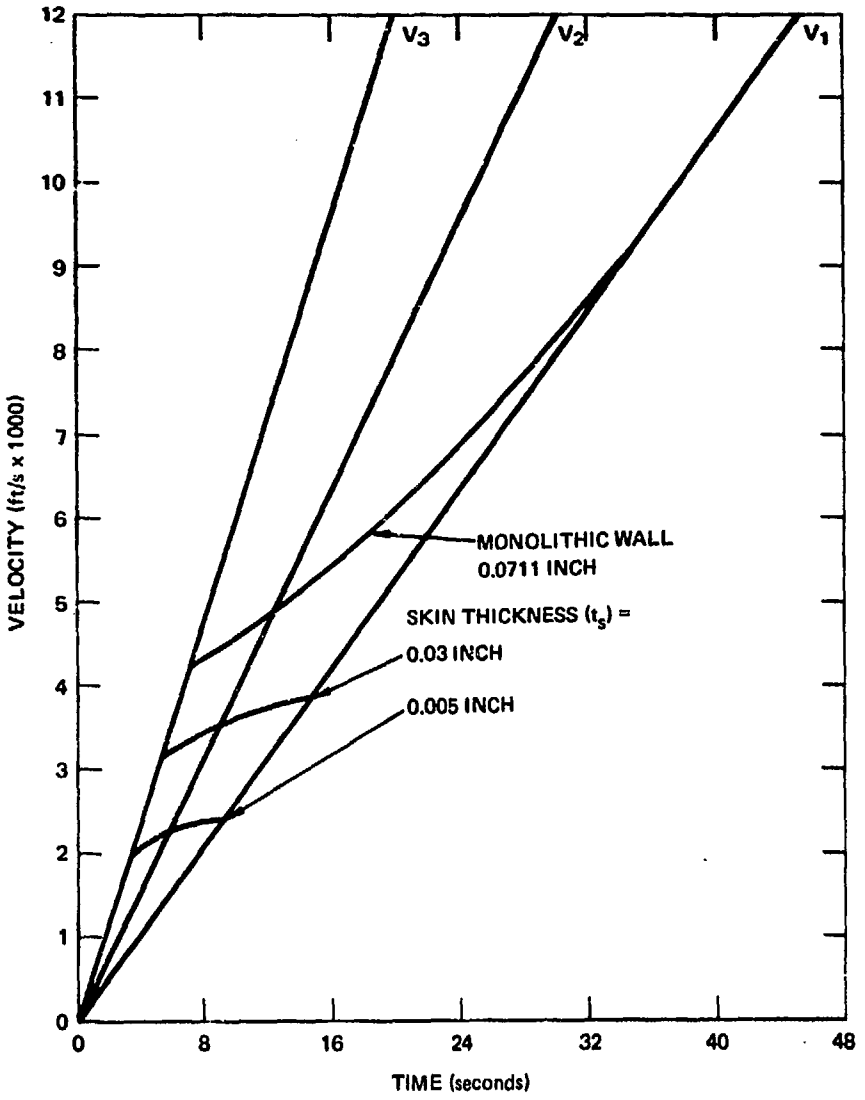

Fig. 26 LIMITATIONS FOR ALUMINA A-SANDWICH WITH 66% POROSITY, QE = 80°, K-BAND RADAR

ratio and specific heat were assumed unaffected and the modulus and conductivity ratios plotted in Figs. 14 and 15 for alumina were assumed to hold for the Pyroceram as well. Reference 10 provided the data values for the dense Pyroceram.

The experience gained from the alumina sandwich work was an aid in selecting the appropriate wall definitions for the Pyroceram. Only two A-sandwich configurations were investigated – one with a thin skin and one with the thickest practical skin. Figure 27 shows the stress versus time data generated for 66% porous Pyroceram designs that were flown at an 80° QE on both V1 and V3. The figure shows much similarity to the stress histories of the alumina sandwiches, that is, all of the sandwich walls show higher stresses than the monolithic designs. Also evident in Figure 27 is a dip in the stress history of the monolithic wall on trajectory V1 at about 16 seconds. This phenomenon is explained by observing that the thermal expansion data for Pyroceram 9606 undergoes a change in slope near 1000°F. This change is probably due to a partial inversion of one of the solid phases of the Pyroceram. Near room temperature, Pyroceram exhibits an expansion rate of around 4.2×10^{-6} in/in-°F; this rate decreases to about 1.6×10^{-6} in/in-°F at 1000°F and then increases again to about 2.8×10^{-6} in/in-°F at higher temperatures. An inspection of the thermal gradient through the monolithic wall at around 16 seconds revealed that the average wall temperature was around 1000°F, indicating that the variable expansion data was causing the anomalous stress history.

Figure 28 presents the velocity limits for the wall definitions analyzed in Fig. 27. As before, the sandwich designs are significantly more limited than the monolithic case.

The similarity between the Pyroceram data and the alumina data leads to the conclusion that there would be no optimum Pyroceram 9606 sandwich parameters. To verify this thought and create further design limits the following cases were examined: X-band, 66% porosity at 20°QE (Fig.

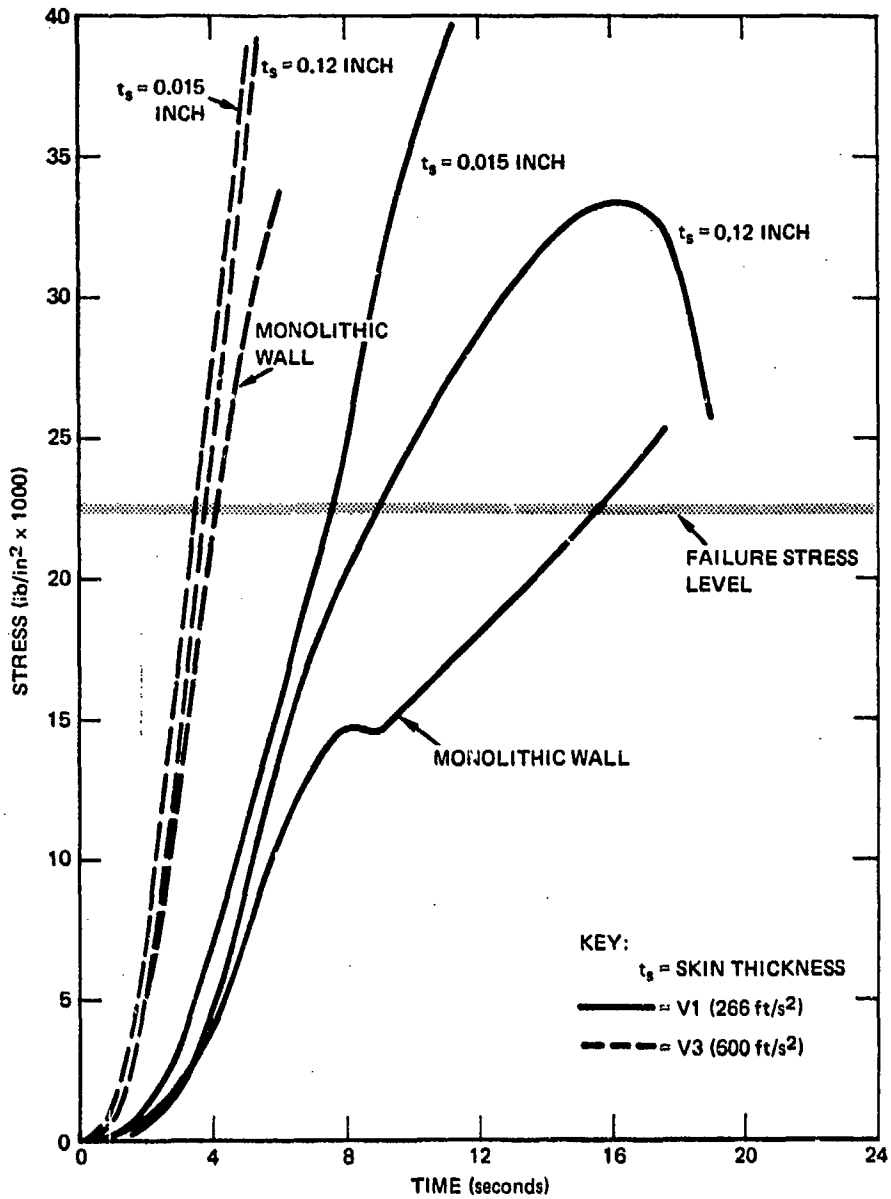

Fig. 27 MAXIMUM STRESS HISTORIES FOR PYROCERAM 9606 X-BAND WALLS WITH 66% POROUS CORE, QE = 80°

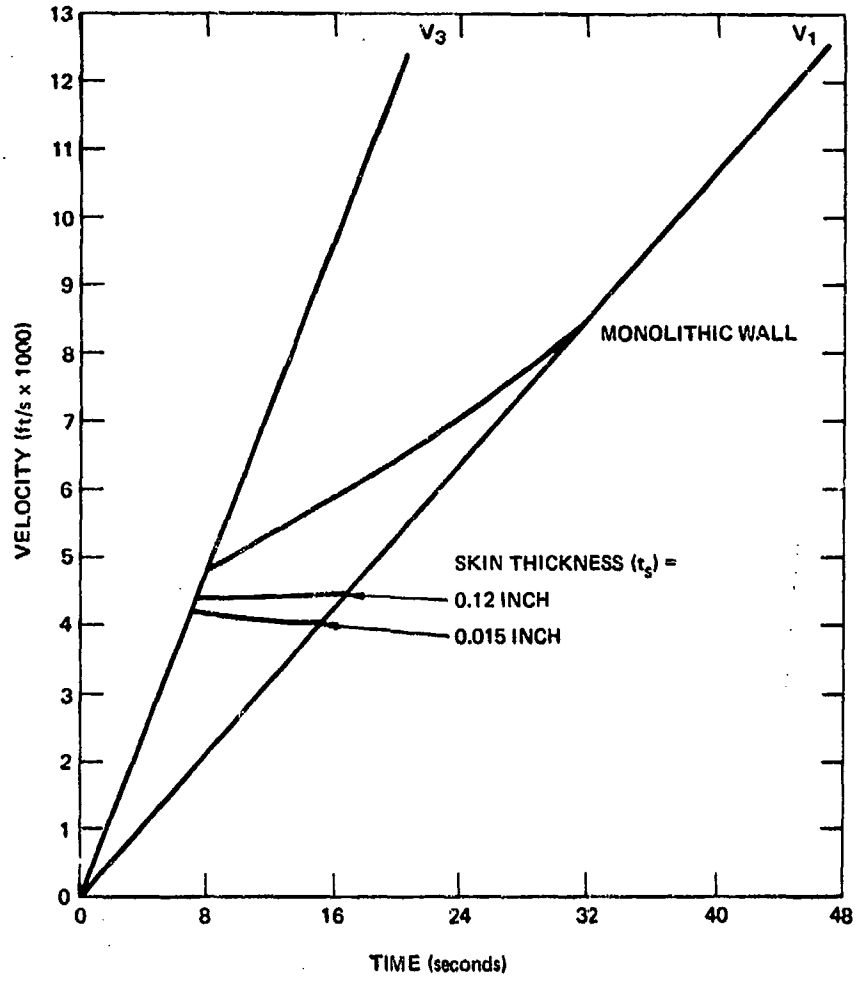

Fig. 28 THERMAL STRESS LIMITATIONS OF PYROCERAM 9606 A-SANDWICH WITH 66% POROUS CORE, X-BAND, QE = 80°

29); K-band, 66% porosity at 80° QE (Fig. 30); and C-band, 66% porosity at 80° QE (Fig. 31).

The results (shown in Figs. 29 through 31) indicate the same general conclusion as noted for the alumina sandwich walls: no case studied provided better performance than the monolithic wall design. In the cases where the Pyroceram monolithic and A-sandwich designs were equally limited, the limitation was caused by melting rather than thermal stress. In Fig. 30 it is noted that both the monolithic and A-sandwich walls reach melting limitations at the same time. Thermally, this would appear to be a paradox; the A-sandwich wall, having the low conductivity core, would be expected to achieve higher temperatures than the monolithic "sink." In fact, at K-band the monolithic wall is quite thin (0.08 inch) and represents very little thermal capacity. The 0.04 inch skin A-sandwich also has 0.08 inch of solid wall plus some core material and therefore represents a somewhat larger thermal capacity, lengthened the time required to reach a particular overall temperature. The sandwich construction clearly exhibits lower flight limits with the majority of the Pyroceram failures occurring below Mach 4.5. A complete skin thickness survey was not made at each differing condition because the trends noted in the previous alumina and Pyroceram work indicated no variations.

COMBINED LIMITS OF A-SANDWICH STRUCTURES

The discussion of limitations of A-sandwich structures has so far included only thermal stress. In the preceding paragraphs, mention is made of limitations due to melting, which suggests that there may be some other factors besides thermal stress failure which would render a radome inoperable. A full definition of a radome's limitations would include effects due to melting, aerodynamic pressures, maneuver accelerations, and electrical degradation due to the temperature dependence of the dielectric constant.

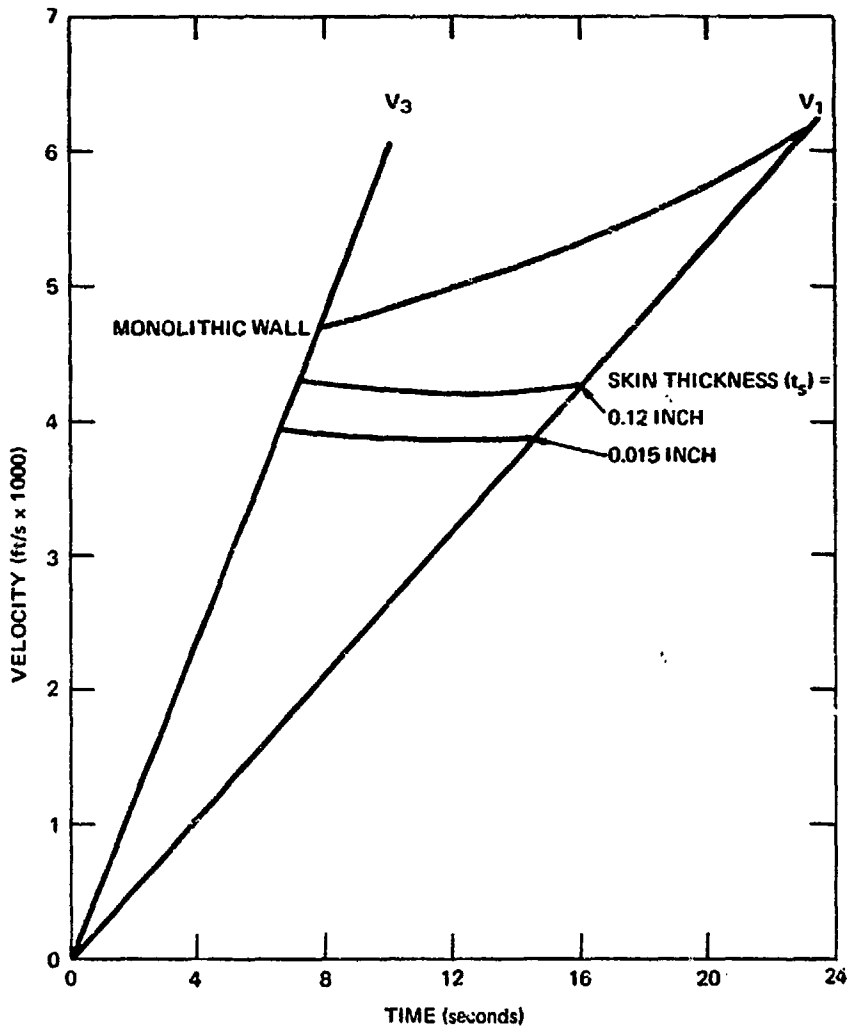

Fig. 29 THERMAL STRESS LIMITATIONS OF PYROCERAM 9606 A-SANDWICH WITH 66% POROUS CORE, X-BAND, $\theta E = 20^{o}$

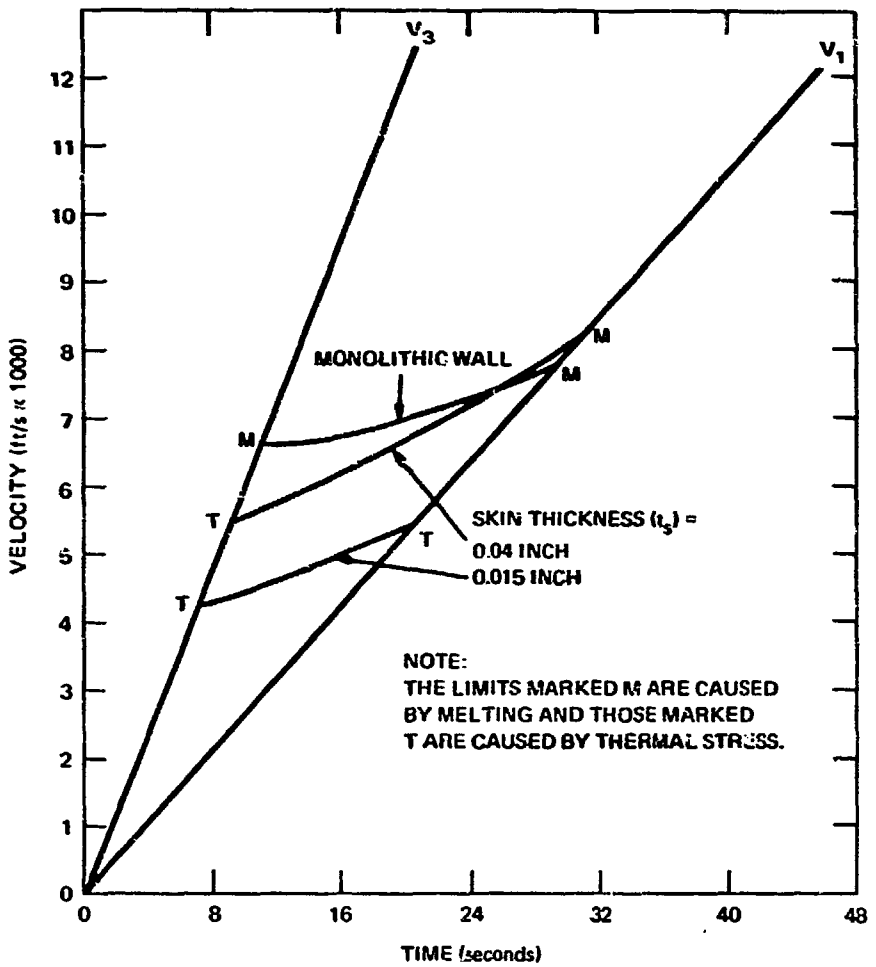

Fig. 30 THERMAL STRESS LIMITATIONS OF PYROCERAM 9606 A-SANDWICH WITH 66% POROUS CORE, K-BAND, QE = 80°

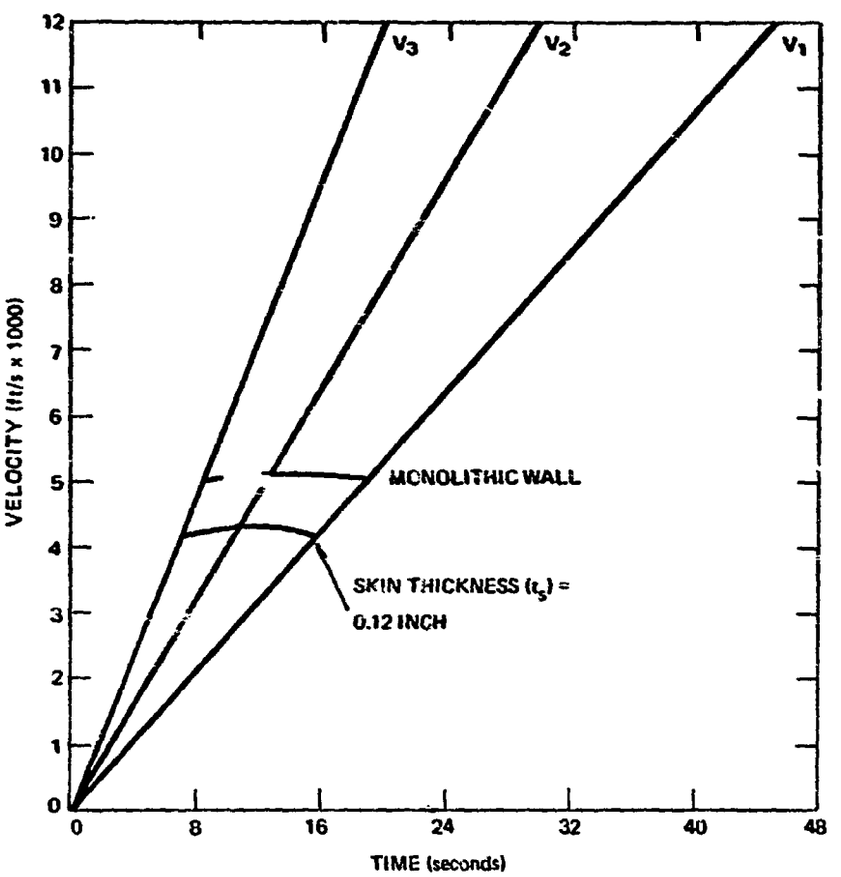

Fig. 31 THERMAL STRESS LIMITATIONS OF PYROCERAM 9606 A-SANDWICH WITH 66% POROUS CORE, C-BAND, QE = 80°

For monolithic alumina and Pyroceram 9606 the mechanical load limitations as defined in Ref. 23 were found to always be in excess of the thermal stress or electrical limits, that is, the thermal stress or electrical limits were always the controlling factors. Since the A-sandwich wall thicknesses for these materials is greater and the thermal stress limits are lower than the monolithic wall cases, the a priori conclusion can be stated that mechanical loads will not be the limiting parameter for the materials considered here.

When considering the electrical limitations of A-sandwich designs, the results from monolithic design studies cannot be as readily applied. The A-sandwich, with its low density core, is electrically more complicated than half-wave monolithic wall owing mainly to internal reflections at each skin core interface and the two different dielectric constants present. A brief search of the literature has not revealed any precise way of analyzing the boresight error rates associated with temperature changes through the A-sandwich wall. Only the following qualitative observations can be made.

In the previous monolithic radome limits study (Ref. 23), electrical limitations were the lowest limitations for some of the trajectories studied, but in general the limits for Pyroceram and alumina were those imposed by either thermal stress or melting. The current study has shown the thermal stress limitations of A-sandwich radome designs to be considerably below that found for comparable monolithic designs. Furthermore, an inspection of the temperature gradient across an A-sandwich wall will reveal that at the time of thermal stress failure, a significant temperature increase has been experienced by only the outer skin and a small portion of the core. Consequently, it is felt that any changes in electrical properties due to temperature would be restricted to this thin outer layer of the sandwich and hence boresight errors would be small enough to be tolerable. On the basis of these observations and in the absence of any electrical scheme for quantitative measurements, it is condluced that the electrical limitations for A-sandwich radomes are superseded by the thermal stress susceptibility of the design.

6. CONCLUSIONS

The study of thermal stresses in A-sandwich ceramic shells of revolution presented in this report has shown the inherent susceptibility of A-sandwich structures to thermal stress. Moreover, a method for theoretically predicting A-sandwich thermal stresses has been validated and then used to define the thermal stress limitations of alumina and Pyroceram 9606 radomes on supersonic flights. The computer methods that were developed for the limitations study are quite general and could be used for any properly defined material.

Although every possible flight environment was not investigated, the cases which were studied encompassed the maximum and minimum bounds. Similarly, every possible A-sandwich design was not tried but the cases that were examined are felt to be representative of A-sandwich performance and accurately describe the major tendencies of A-sandwich design under thermal stress.

REFERENCES

1. "Properties of Ceramic A-Sandwich Alumina Materials," Glen Dale Research Center, INTERPACE, May 27, 1964.

2. D. L. Loyet and R. Yoshitani, "Ceramic Sandwich Radome Design," 1964 Proceedings of the OSU-RTD Symposium on Electromagnetic Windows, Volume 3, May 25, 1964.

3. D. L. Loyet, "Development of an A-Sandwich Radome for the AIM-54A Missile," Report 2783 3/217, Hughes Aircraft Co., February 4, 1964.

4. R. L. Copeland and R. F. Greene, "Fabrication Techniques for Lightweight Hyper-environment Windows," Technical Report AFAL-TR-67-238, October 1967.

5. R. M Rivello, Thermal Stress Analysis of Sandwich Cylinders, APL/JHU TG 721, August 1965.

6. D. W. Fox, H. Shaw and J. Jellinek, "Numerical Approximations in Heat Transfer Problems and Usage of IBM 7094 Computer for Solutions," APL/JHU CF-2954, May 1962.

7. L. A. Barber, D. W. Conn, and R. W. Newman, "A Guide to the Usage of the Standard Heat Transfer Program (PL/1)," APL/JHU BCP-441 R1, August 1969.

8. R. O. Weiss, The Thermal Stresses in a Thick-Walled Cone by the Method of Finite Differences, APL/JHU TG 914, May 1967.

9. T. Eck, "Determination of Certain Physical and Mechanical Properties of the Alumina Used in the Sandwich Test Cylinders," APL/JHU EM-4130, September 1967.

Preceding page blank

REFERENCES (cont'd)

10. L. B. Weckesser and D. L. Coble, "Electrical, Mechanical and Thermal Properties of Alumina, Fused Silica and Pyroceram 9606," APL/JHU EM-3926, December 7, 1964.

11. T. E. Tice (ed), Techniques for Airborne Radome Design, Air Force Avionics Laboratory, Wright-Patterson AFB, Technical Report AFAL-TR-66-391, Vol. I, December 1966.

12. R. L. Coble and W. C. Kingery, "Effect of Porosity on Physical Properties of Sintered Alumina," Journal of the American Ceramic Society, Vol. 39, No. 11, November 1956, pp. 377-285.

13. J. B. Austin, "Thermal Expansion of Nonmetallic Crystals," ibid, Vol. 35, No. 10, October 1952, pp. 243-253.

14. J. W. Kelly, and J. F. Whatham, The Temperature and Porosity Dependence of the Modulus of Rigidity and Poisson's Ratio of Beryllia, Australian Atomic Energy Commission Research Establishment.

15. R. M. Spriggs, "Expression for Effect of Porosity on Elastic Modulus of Polycrystalline Refractory Materials Particularly Aluminum Oxide," Journal of American Ceramic Society, Vol. 44, No. 12, December 1961, pp. 628-629.

16. F. P. Knudsen, "Effect of Porosity on Young's Modulus of Alumina," Journal of American Ceramic Society, Vol. 45, No. 2, Febrary 1962, pp. 94-95.

17. F. P. H. Hasselman, "On the Porosity Dependence of the Elastic Moduli of Polycrystalline Refractory Materials," Journal of the American Ceramic Society, Vol. 45, No. 9, December 1962, pp. 452-3.

18. Z. Hashin, "Elastic Moduli of Hetergeneous Materials," Journal of Applied Mechanics, Vol. 29, No. 1, 1962, pp. 143-150.

REFERENCES (cont'd)

19. J. K. MacKenzie, "Elastic Constants of a Solid Containing Spherical Holes," Proceedings of the Physics Society (London), Vol. 63B, No. 1, 1950, pp. 2-11.

20. J. D. McClelland and L. O. Petersen, "The Effect of Porosity on the Thermal Conductivity of Alumina," Atomics International, Canoga Park, Calif., U.S. Atomic Energy Commission Report NAA-SR-6473, 1961.

21. C. M. Pyron, Jr. and C. D. Pears, "The Mechanisms of Heat Transfer Through Porous Materials at Elevated Temperatures," Paper #65-HT-46, American Society of Mechanical Engineers.

22. A. L. Loeb, "Thermal Conductivity: VIII, A Theory of Thermal Conductivity of Porous Materials," Journal of the American Ceramic Society, Vol. 37, No. 2, pp. 96-99.

23. L. B. Weckesser, R. H. Hallendorff, and R. P. Suess, Environmental Limitations of Alumina, Fused Silica and Pyroceram 9606 Radomes, APL/JHU TG 865, May 1967.

24. M. P. Bleday and M. A. St John, "Allowable Velocity Histories of Ceramic Radomes," presented at 9th AIAA/ASME Structural Dynamics and Materials Conference, April 1968, Palm Springs, Calif., April 1968, p. 212.

ACKNOWLEDGMENTS

The author wishes to acknowledge the valuable help of Louis B. Weckesser during the course of this investigation. His able guidance and careful insights have added much to the content of this report. Also Oscar Seidman and Lionel Pasiuk of NavOrd 035 are acknowledged for their support of this investigation.